

NASA TECHNICAL NOTE



NASA TN D-2780

NASA TN D-2780



**BLUNT BODY SOLUTIONS FOR
SPHERES AND ELLIPSOIDS
IN EQUILIBRIUM GAS MIXTURES**

*by Mamoru Inouye
Ames Research Center
Moffett Field, Calif.*



BLUNT BODY SOLUTIONS FOR SPHERES AND ELLIPSOIDS
IN EQUILIBRIUM GAS MIXTURES

By Mamoru Inouye

Ames Research Center
Moffett Field, Calif.

NATIONAL AERONAUTICS AND SPACE ADMINISTRATION

For sale by the Clearinghouse for Federal Scientific and Technical Information
Springfield, Virginia 22151 - Price \$2.00

BLUNT BODY SOLUTIONS FOR SPHERES AND ELLIPSOIDS
IN EQUILIBRIUM GAS MIXTURES

By Mamoru Inouye
Ames Research Center

SUMMARY

An inverse method was used to calculate the flow field in the nose region of blunt bodies traveling at supersonic speeds in equilibrium mixtures of gases that may be present in other atmospheres. Calculations were made for air, nitrogen, carbon dioxide, argon, and a mixture composed of 50-percent argon, 40-percent nitrogen, and 10-percent carbon dioxide. Speeds from 10,000 to 70,000 ft/sec are covered for free-stream densities of 10^{-1} , 10^{-3} , and 10^{-5} times earth sea-level values. Correlations are presented for the shock stand-off distance, surface pressure distribution, and stagnation-point velocity gradient.

INTRODUCTION

The numerical calculation of flow properties in the nose region of blunt bodies traveling at supersonic speeds is described in reference 1 for a perfect gas and for air in thermodynamic equilibrium. The inverse method is used; that is, a shock-wave shape is assumed, and the resulting body shape is calculated. Discovery of a one-parameter family of shock-wave shapes that will produce spheres and ellipsoids to close accuracy in effect permits a direct solution to the problem.

In the present report the calculations reported in reference 1 are extended to include equilibrium mixtures of gases present in other atmospheres. Solutions have been obtained for air, nitrogen, carbon dioxide, argon, and a mixture composed of 50-percent argon, 40-percent nitrogen, and 10-percent carbon dioxide. Speeds from 10,000 to 70,000 ft/sec have been considered for free-stream densities and pressures of 10^{-1} , 10^{-3} , and 10^{-5} times earth sea-level values. The free-stream temperature was thus maintained constant for each gas at such a level that the free-stream gas was undissociated. Results for the shock-wave shape parameter, standoff distance, surface pressure distribution, and stagnation-point velocity gradient are shown together with a tabulation of stagnation-point and shock-wave conditions.

SYMBOLS

- A₅ shock-wave shape parameter (see eq. (1))
A₇ shock-wave shape parameter (see eq. (2))

a speed of sound
 B_b body bluntness parameter, $(b/c)^2$
 b,c semimajor and semiminor axes of ellipsoid
 h enthalpy
 M Mach number
 p pressure
 R_b radius of curvature of the body for $y = 0$
 R_s radius of curvature of the shock wave for $y = 0$
 s distance along the surface measured from the stagnation point
 T temperature
 V velocity
 $X(y)$ shock-wave shape
 x,y cylindrical coordinates with origin on shock wave and $R_s = 1$
 γ isentropic exponent, $a^2\rho/p$
 Δ shock standoff distance
 ρ density
 ρ_0 earth sea-level density, 0.002377 slug/ft³

Subscripts

∞ free-stream conditions
 2 conditions behind normal shock
 st stagnation point on body

CALCULATION METHOD

Blunt-Body Solution

The inverse method is used for calculating the flow field around blunt-nosed axisymmetric bodies. The partial differential equations governing steady, inviscid flow of a gas in thermodynamic equilibrium are integrated by a finite-difference technique proceeding from an assumed shock-wave shape to the corresponding body shape. Iteration of the shock-wave shape is usually necessary to obtain the desired body shape, which is normally a conic section. Details of the numerical analysis and solutions for perfect gases and air in thermodynamic equilibrium are presented in reference 1. The changes made to obtain the present results are the extension to arbitrary equilibrium gas mixtures and a slight modification of the shock-wave shape as described in the following sections.

Thermodynamic Properties

Thermodynamic properties for various gases have been calculated by Dr. Harry E. Bailey of Ames Research Center following the assumptions and approximations made in reference 2. The properties for carbon dioxide are reported in reference 3. The data cover temperatures to $45,000^{\circ}$ R and densities from 10^{-7} to 10^{+3} times a reference density based on a temperature of 491.7° R and a pressure of 1 atmosphere. The gases considered in this study are air, nitrogen, carbon dioxide, argon, and a mixture composed of 50-percent argon, 40-percent nitrogen, and 10-percent carbon dioxide. The domain of the thermodynamic data in a pressure-density plane is shown in figure 1. The boundaries are slightly different for the various gases.

For use in the blunt-body program, the calculated thermodynamic data have been spline fitted with cubics by the method described in reference 4, the coefficients being stored on magnetic tape for the various gas mixtures. Aside from the shock-wave relations which require the enthalpy, the blunt-body solution requires only the speed of sound as a function of pressure and density. Values for the speed of sound and enthalpy obtained from the curve fits have been checked and found to agree with the original data within 1 percent, except for small regions where differences as high as 5 percent occur. At low temperatures perfect gas relationships are used with the appropriate values of the gas constant and ratio of specific heats.

Shock-Wave Shape

The success of the inverse method depends on being able to define a simple shock-wave shape that will produce spherical and ellipsoidal bodies to close accuracy. It was found in reference 1 that the shock shape given by the rational polynomial

$$X(y) = \frac{0.5y^2 + A_5y^4}{2A_5y^3} \quad (1)$$

$\frac{1}{2} C^{(2)}$ M_∞^2
 $\frac{1}{2} C^{(1)}$ $\sqrt{M_\infty^2 - 1}$ $C^{(4)}$

is successful in this regard. It was possible by varying the single parameter, A_5 , to obtain spheres and ellipsoids over a wide range of free-stream conditions for perfect gases and air in thermodynamic equilibrium. One might expect similar success for other gases. However, the shock shape given by equation (1) does not have even symmetry about $y = 0$ because of the y^3 term in the denominator. This defect did not cause any numerical difficulties in reference 1, probably because of the smoothing procedure employed. A simple change eliminates this objectionable behavior and yields essentially the same shock shape. If equation (1) is squared and the denominator is altered so that X varies linearly with y for large values of y , there results

$$[X(y)]^2 = \frac{0.25y^4 + A_7y^6}{1 + \frac{4A_7y^4}{M_\infty^2 - 1}} \quad (2)$$

with the single parameter, A_7 , which is the seventh term in the numerator polynomial. Comparison with equation (1) shows that $A_7 \sim A_5$ provided A_5 is small, which is true for spheres (~ 0.1). A few test cases showed that the results for spheres found in reference 1 could be reproduced with the shock shape given by equation (2).

RESULTS AND DISCUSSION

Spheres

The flow field around a spherical nose has been calculated for the following gases: air, nitrogen, carbon dioxide, argon, and a mixture composed of 50-percent argon, 40-percent nitrogen, and 10-percent carbon dioxide. The free-stream conditions selected were densities and pressures equal to 10^{-1} , 10^{-3} , and 10^{-5} times the earth sea-level value and velocities from 10,000 to 70,000 ft/sec, the upper limit being determined by the maximum temperature of $45,000^\circ$ R. It is recognized that for some of the cases studied (at the highest velocities and lowest densities), the assumption of inviscid, equilibrium flow may be violated. However, these results are included to serve as reference values for assessing the effects of nonequilibrium flow when such calculations are available.

The output from a blunt body solution includes the coordinates of the shock wave and sonic line, and the flow properties on the body and in the shock layer including those on a line joining the body and shock in the supersonic region. The latter data can be used as input to a method of

characteristics program to continue the solution downstream over an afterbody of arbitrary shape. A résumé of the solutions is presented in table I. In the following paragraphs, there are presented results and correlations that are useful for the calculation of radiative and convective heating to spherical noses.

Values of the shock-wave shape parameter, A_7 , required in equation (2) to produce spherical noses are shown in figure 2 for the gases studied. The effect of changes in the free-stream velocity on the shock shape is generally greater than the effect of changes in the free-stream density. However, in regions where dissociation and ionization are occurring, the shock parameter changes drastically.

The ratio of shock standoff distance, Δ , to the radius of curvature of the shock at the axis of symmetry, R_s , is shown in figure 3(a) for all the gases as a function of the density ratio across the normal shock, ρ_∞/ρ_2 . There is no significant effect of gas composition on this ratio; moreover, good agreement is observed with the constant-density solution of Hayes and Probstein (ref. 5) given by the following equation:

$$\frac{\Delta}{R_s} = \frac{\rho_\infty/\rho_2}{1 + \sqrt{8\rho_\infty/3\rho_2}} \quad (3)$$

(The values of Δ/R_s for argon at 10,000 ft/sec are not shown because they exceed 0.11; however, they are also correlated by eq. (3).) The dependence of the standoff distance on the density ratio can be explained on the basis of mass conservation. If the density behind the shock increases, the standoff distance must decrease in order for the mass flow away from the stagnation point in the shock layer to remain nearly the same.

The designer is more interested in knowing the standoff distance in terms of the nose radius, R_b , as shown in figure 3(b). The results from the present numerical solutions for $0.04 < \rho_\infty/\rho_2 < 0.16$ can be correlated by a straight line defined by

$$\frac{\Delta}{R_b} = 0.78 \frac{\rho_\infty}{\rho_2} \quad (4)$$

This correlation was originally obtained by Seiff (ref. 6) from a collection of experimental and theoretical results for air and perfect gases. Since the constant-density solution (ref. 5) does not yield the nose radius, it is necessary to assume, for example, that the shock and body are concentric in order to relate the standoff distance to the nose radius. This assumption is not valid as shown in figure 3(b).

The variation of standoff distance with free-stream velocity and density for each of the gases considered is shown in figure 4. The symbols represent results from the present numerical solutions, and the curves represent the simple linear law of equation (4). The latter curves require solution of the normal shock relations for an equilibrium gas, a calculation that requires

much less effort than a blunt body solution. Since the standoff distance is just a linear function of the density ratio, the curves of figure 4 actually represent the variation of the density ratio across a normal shock with free-stream velocity and density. It is to be noted that for a perfect gas the density ratio approaches a limiting value equal to $(\gamma - 1)/(\gamma + 1)$ as the Mach number becomes infinite. For a real gas the density ratio decreases with increasing free-stream velocity and decreasing free-stream density as dissociation and ionization produce more particles per unit volume behind the shock. When the chemical composition does not change appreciably, the density ratio remains nearly constant. The curves for standoff distance in figure 4, in general, reflect this behavior.

The ratio of R_b to R_s for the present numerical solutions is shown as a function of the density ratio in figure 5. Combining equations (3) and (4) yields the following correlation equation:

$$\frac{R_b}{R_s} = \frac{1.28}{1 + \sqrt{8\rho_\infty/3\rho_2}} \quad (5)$$

For a perfect gas the results of reference 1 show that the surface pressure (normalized by the stagnation-point pressure) in the subsonic region of a spherical nose has nearly the same distribution for all Mach numbers greater than about 10. In addition, the surface pressure distributions show little dependence on γ as shown in figure 6 for $M_\infty = 30$. These results can be correlated by equation (6)

$$\frac{p}{p_{st}} = 1.0 - 1.25 \sin^2\left(\frac{s}{R_b}\right) + 0.284 \sin^4\left(\frac{s}{R_b}\right) \quad (6)$$

which yields values of the pressure between the predictions of modified Newtonian theory with and without the centrifugal correction. The surface pressure distributions for all the gases and free-stream conditions considered in the present study are also correlated by this equation. A typical set of results is shown in figure 7 for $\rho_\infty/\rho_0 = 10^{-1}$ and for V_∞ from 10,000 to 50,000 ft/sec. However, if one is interested in the pressure gradient along the surface, equation (6) may be inadequate, and the exact blunt body solution should be used.

The velocity distribution along the surface in the subsonic region is nearly linear for the present results as exemplified in figure 8 for the specified mixture of argon, nitrogen, and carbon dioxide. Thus the stagnation-point velocity gradient, which is required for calculating the heating rate, describes the velocity distribution in the subsonic region. According to Newtonian theory, the velocity gradient at the stagnation point is given by the following equation:

$$\frac{dV}{ds} = \frac{1}{R_b} \sqrt{\frac{2p_{st}}{\rho_{st}}} \quad (7)$$

The results from the present solutions are as much as 15 percent higher than Newtonian theory (ordinate equal to unity) as shown in figure 9. The following equation, which has the form given by the constant-density solution of reference 5, correlates the present results as a function of the density ratio across a normal shock:

$$\frac{R_b \frac{dV}{ds}}{\sqrt{\frac{2p_{st}}{\rho_{st}}}} = \frac{1.187}{1 + 0.225 \sqrt{\frac{\rho_{\infty}}{\rho_2}}} \quad (8)$$

Since the flow is isentropic along the surface, the density distribution can be calculated from the previously described pressure distribution and the enthalpy distribution, which is obtained from the velocity distribution using the equation

$$h = h_{st} - \frac{V^2}{2} \quad (9)$$

For subsonic flow the kinetic energy is only a small fraction of the total energy, so the enthalpy is nearly constant. Hence, the density distribution depends primarily on the pressure distribution which is given by equation (6).

Ellipsoids

The flow field around prolate and oblate ellipsoids can be found with the same procedure as for a sphere. For example, ellipsoids with values of the body bluntness from zero (a paraboloid) to 2.25 have been found for the previously specified mixture of argon, nitrogen, and carbon dioxide for free-stream velocities from 10,000 to 50,000 ft/sec and for a free-stream density of 10^{-3} times the earth sea-level density. A résumé is presented in table II. The shock shape parameter varies nearly linearly with body bluntness as shown in figure 10. This behavior was also shown in reference 1 for air. A similar dependence of shock shape parameter on body bluntness is to be expected for other gases.

The shock standoff distance expressed in terms of the shock radius, R_s , is not a function of the body bluntness for constant free-stream conditions. However, the body size, characterized by its radius of curvature at the stagnation point, R_b , increases with body bluntness so that the ratio, Δ/R_b , decreases slightly with increasing body bluntness as shown in figure 11. The stagnation-point velocity gradient expressed in dimensionless form as shown in figure 12 increases slightly with body bluntness.

The present results can be applied to determine the effect of nose bluntness on the flow field around a family of ellipsoids with the same base radius. For an ellipsoid, the ratio of the radius of curvature at the stagnation point to the base radius is equal to the square root of the body bluntness. Therefore, as the body bluntness increases, the shock standoff distance would increase and the stagnation-point velocity gradient would decrease.

SUMMARY OF RESULTS

The flow of an equilibrium gas around spheres has been calculated numerically by an inverse method for various gases over a wide range of free-stream conditions. The following results have been obtained:

1. The shock-wave shapes for spherical bodies can be expressed by a one-parameter rational polynomial.
2. The ratio of the shock standoff distance to the nose radius is a linear function of the density ratio across a normal shock.
3. A simple trigonometric expression has been found to correlate the surface pressure distribution in the subsonic region of spheres for all the gases and free-stream conditions considered in the present study.
4. The stagnation-point velocity gradient can be expressed as a function of the density ratio across a normal shock.
5. The present method can be used to calculate the flow field around prolate and not too blunt oblate ellipsoids.

Ames Research Center
National Aeronautics and Space Administration
Moffett Field, Calif., Feb. 15, 1965

REFERENCES

1. Lomax, Harvard; and Inouye, Mamoru: Numerical Analysis of Flow Properties About Blunt Bodies Moving at Supersonic Speed in an Equilibrium Gas. NASA TR R-204, 1964.
2. Marrone, Paul V.: Inviscid, Nonequilibrium Flow Behind Bow and Normal Shock Waves, Part I. General Analysis and Numerical Examples. CAL Rep. QM-1626A-12(I), May 1963.
3. Bailey, H. E.: Thermodynamic Properties of Carbon Dioxide. NASA SP-3014, 1965.
4. Walsh, J. L.; Ahlberg, J. H.; and Nilson, E. N.: Best Approximation Properties of the Spline Fit. J. Math. Mech., vol. 11, no. 2, Mar. 1962, pp. 225-234.
5. Hayes, Wallace D.; and Probst, Ronald F.: Hypersonic Flow Theory. Academic Press, New York, 1959, pp. 158-162.
6. Seiff, Alvin: Recent Information on Hypersonic Flow Fields in Gas Dynamics in Space Exploration. NASA SP-24, 1962.

TABLE I.- RESUME OF SOLUTIONS FOR SPHERES

Free-stream conditions						Air						Shock-wave conditions			
P_{∞}/P_0	$P_{\infty}'/lb/ft^2$	$\rho_{\infty}'/slugs/ft^3$	T_{∞}'/OR	$V_{\infty}'/ft/sec$	M_{∞}	$P_{st}, lb/ft^2$	$P_{st}'/slugs/ft^2$	T_{st}'/OR	γ_{st}	$\eta_{st}, ft^2/sec^2$	A_7	R_b/R_s	Δ/R_s	Δ/R_b	ρ_{∞}/ρ_2
10 ⁻¹	211.6	.2377-s	513.9	10,000	8.949	0.2254+s	0.2013-z	6,265	1.191	0.5311+s	0.0743	0.7848	0.0760	0.0994	0.1253
				20,000	17.90	.9124+s	.2827-z	13,810	1.169	.2031+s	.0952	.8438	.0585	.0693	.0876
				30,000	26.85	.2064+e	.3325-z	19,480	1.217	.4531+e	.1001	.8815	.0510	.0579	.0739
				40,000	35.80	.3654+e	.3013-z	31,280	1.252	.8031+z	.1199	.8777	.0557	.0634	.0817
				50,000	44.74	.5701+e	.2935-z	41,000	1.276	.1253+10	.1077	.8753	.0569	.0650	.0839
10 ⁻³	2.116	.2377-s	513.9	10,000	8.949	.2270+s	.2253-z	5,439	1.147	.5311+s	.0696	.7942	.0707	.0891	.1113
				20,000	17.90	.9191+s	.3379-z	11,040	1.129	.2031+s	.0955	.8613	.0501	.0582	.0728
				30,000	26.85	.2076+e	.3940-z	15,560	1.221	.4531+e	.1011	.9070	.0441	.0486	.0620
				40,000	35.80	.3684+e	.3747-z	23,740	1.178	.8031+e	.1172	.8894	.0459	.0516	.0653
				50,000	44.74	.5759+e	.3837-z	28,910	1.198	.1253+10	.1117	.8951	.0450	.0503	.0637
10 ⁻⁵	.02116	.2377-r	513.9	10,000	8.949	.2286+1	.2576-e	4,640	1.118	.5311+s	.0701	.8123	.0631	.0776	.0967
				20,000	17.90	.9244+1	.3993-e	9,094	1.106	.2031+s	.1004	.8771	.0433	.0494	.0613
				30,000	26.85	.2084+e	.4451-e	13,410	1.213	.4531+e	.1044	.9286	.0397	.0427	.0547
				40,000	35.80	.3706+e	.4588-e	18,630	1.133	.8031+e	.1173	.9018	.0384	.0426	.0531
				50,000	44.74	.5799+e	.4852-e	21,710	1.150	.1253+10	.1172	.9111	.0366	.0402	.0501
10 ⁻¹	211.6	.2377-s	499.5	10,000	8.945	.2231+s	.1740-z	7,195	1.280	.5311+s	.0801	.7800	.0888	.1138	.1458
				20,000	17.89	.9131+5	.2880-z	14,430	1.152	.2031+e	.0857	.8408	.0575	.0684	.0860
				30,000	26.84	.2069+e	.3536-z	19,040	1.190	.4531+e	.1026	.8829	.0483	.0547	.0694
				40,000	35.78	.3665+e	.3245-z	29,290	1.247	.8031+e	.1188	.8892	.0522	.0587	.0757
				50,000	44.73	.5713+e	.3083-z	39,310	1.271	.1253+10	.1120	.8822	.0546	.0619	.0798
10 ⁻³	2.116	.2377-s	499.5	10,000	8.945	.2234+s	.1766-z	7,076	1.241	.5311+s	.0878	.7729	.0874	.1130	.1438
				20,000	17.89	.9200+3	.3472-z	11,400	1.121	.2031+e	.0921	.8619	.0489	.0567	.0708
				30,000	26.84	.2082+e	.4298-z	14,670	1.175	.4531+e	.1064	.9048	.0408	.0451	.0567
				40,000	35.78	.3690+e	.3954-z	22,730	1.175	.8031+e	.1235	.8965	.0438	.0489	.0618
				50,000	44.73	.5767+e	.4004-z	27,970	1.193	.1253+10	.1140	.8993	.0434	.0482	.0610
10 ⁻⁵	.02116	.2377-r	499.5	10,000	8.945	.2241+1	.1855-e	6,704	1.169	.5311+s	.0897	.7629	.0834	.1093	.1370
				20,000	17.89	.9254+1	.4128-e	9,306	1.100	.2031+e	.0997	.8791	.0421	.0478	.0593
				30,000	26.84	.2091+e	.5082-e	11,930	1.187	.4531+e	.1080	.9236	.0352	.0381	.0478
				40,000	35.78	.3710+e	.4779-e	18,090	1.130	.8031+e	.1229	.9067	.0371	.0409	.0509
				50,000	44.73	.5804+e	.5037-e	21,110	1.145	.1253+10	.1190	.9135	.0354	.0388	.0483
10 ⁻¹	211.6	.2377-s	783.9	10,000	9.508	.2316+s	.3460-z	5,301	1.111	.5366+e	.0954	.8630	.0491	.0569	.0711
				20,000	19.02	.9241+5	.3939-z	10,690	1.278	.2037+e	.1065	.9212	.0442	.0480	.0619
				30,000	28.52	.2074+e	.3817-z	18,220	1.190	.4537+e	.1071	.8921	.0452	.0507	.0641
				40,000	38.03	.3662+e	.3186-z	30,240	1.287	.8037+e	.1325	.8939	.0531	.0594	.0771
				50,000	47.54	.5704+e	.2969-z	41,020	1.282	.1254+10	.1158	.8793	.0564	.0641	.0829
10 ⁻³	2.116	.2377-s	784.1	10,000	9.511	.2324+s	.3866-z	4,586	1.090	.5366+e	.0974	.8722	.0445	.0511	.0634
				20,000	19.02	.9262+s	.4245-z	9,633	1.296	.2037+e	.0932	.9547	.0415	.0435	.0573
				30,000	28.53	.2087+e	.4714-z	14,120	1.159	.4537+e	.1110	.9092	.0376	.0413	.0516
				40,000	38.04	.3691+e	.3968-z	22,840	1.204	.8037+e	.1345	.9031	.0438	.0485	.0616
				50,000	47.56	.5760+e	.3849-z	28,940	1.210	.1254+10	.1191	.8979	.0449	.0500	.0635
10 ⁻⁵	.02116	.2377-r	783.9	10,000	9.513	.2333+1	.4334-e	3,983	1.078	.5366+e	.1008	.8821	.0403	.0457	.0564
				20,000	19.02	.9283+1	.4610-e	8,746	1.160	.2037+e	.1155	.9315	.0383	.0411	.0528
				30,000	28.54	.2096+e	.5650-e	11,460	1.136	.4537+e	.1151	.9224	.0320	.0347	.0429
				40,000	38.05	.3713+e	.4920-e	17,630	1.158	.8037+e	.1339	.9145	.0362	.0396	.0494
				50,000	47.56	.5799+e	.4865-e	21,640	1.164	.1254+10	.1246	.9135	.0365	.0400	.0500
10 ⁻¹	211.6	.2377-s	711.4	10,000	8.220	.2110+s	.1032-z	16,320	1.511	.5222+e	.0829	.6672	.1374	.2060	.2567
				20,000	16.44	.8944+s	.1982-z	29,750	1.197	.2022+e	.0601	.7727	.0788	.1020	.1275
				30,000	24.66	.2042+e	.2586-z	39,200	1.246	.4522+e	.0862	.8425	.0633	.0751	.0959
				40,000	32.88	.3662+e	.1110-z	15,180	1.317	.5222+e	.0850	.8439	.0521	.0574	.0724
				50,000	41.10	.5781+e	.3192-z	4,293	1.185	.8022+e	.1415	.8690	.0528	.0608	.0771
10 ⁻³	2.116	.2377-s	711.2	10,000	8.220	.2130+s	.1110-z	15,180	1.317	.5222+e	.0850	.8439	.0521	.0574	.0724
				20,000	16.44	.9071+s	.2513-z	22,720	1.152	.2022+e	.0708	.8122	.0645	.0794	.0992
				30,000	24.66	.2065+e	.3376-z	28,390	1.189	.4522+e	.0965	.8732	.0502	.0576	.0728
				40,000	32.88	.3662+e	.3192-z	4,293	1.185	.8022+e	.1415	.8690	.0528	.0608	.0771
				50,000	41.10	.5781+e	.4345-e	39,550	1.157	.1252+10	.1082	.8996	.0403	.0448	.0561
10 ⁻⁵	.02116	.2377-r	711.5	10,000	8.221	.2160+1	.1251-e	13,510	1.180	.5222+e	.0845	.6597	.1138	.1779	.2121
				20,000	16.44	.9159+1	.3093-e	18,070	1.117	.2022+e	.0810	.8416	.0540	.0641	.0799
				30,000	24.66	.2081+e	.4237-e	21,870	1.150	.4522+e	.1054	.8948	.0412	.0461	.0576
				40,000	32.88	.3689+e	.3915-e	34,090	1.137	.8022+e	.1323	.8841	.0441	.0499	.0625
				50,000	41.10	.5781+e	.4345-e	39,550	1.157	.1252+10	.1082	.8996	.0403	.0448	.0561
50-percent argon, 40-percent nitrogen, 10-percent carbon dioxide															
10 ⁻¹	211.6	.2377-s	633.6	10,000	8.749	.2246+s	.1903-z	7,787	1.304	.5270+e	.0668	.8014	.0824	.1028	.1323
				20,000	17.50	.9127+s	.2850-z	16,120	1.194	.2027+e	.0866	.8494	.0581	.0684	.0868
				30,000	26.25	.2049+e	.2789-z	29,210	1.233	.4527+e	.1162	.8601	.0594	.0691	.0887
				40,000	34.99	.3647+e	.2895-z	39,400	1.258	.8027+e	.1020	.8676	.0576	.0663	.0852
				50,000	43.74	.5739+e	.3456-z	37,980	1.323	.1253+10	.0965	.9132	.0496	.0543	.0708
10 ⁻³	2.116	.2377-s	633.5	10,000	8.749	.2255+s	.2019-z	7,235	1.320	.5270+e	.0762	.8250	.0786	.0952	.1241
				20,000	17.50	.9201+s	.3478-z	12,690	1.165	.2027+e	.0931	.8726	.0489	.0561	.0706
				30,000	26.25	.2067+e	.3440-z	22,590	1.167	.4527+e	.1112	.8749	.0494	.0565	.0714
				40,000	35.00	.3684+e	.3763-z	28,080	1.191	.8027+e	.1075	.8900	.0457	.0514	.0649
				50,000	43.74	.5739+e	.3456-z	37,980	1.323	.1253+10	.0965	.9132	.0496	.0543	.0708
10 ⁻⁵	.02116	.2377-r	633.6	10,000	8.746	.2263+1	.2134-e	6,813	1.220	.5270+e	.1350	.8175	.0746	.0912	.1175
				20,000	17.49	.9254+1	.4133-e	10,410	1.152	.2027+e	.0964	.8928	.0421	.0472	.0591
				30,000	26.24	.2080+e	.4187-e	17,870	1.126	.4527+e	.1124	.8896	.0416	.0468	.0584
				40,000	34.98	.3710+e	.4734-e	21,310	1.145	.8027+e	.1148	.9068	.0374	.0412	.0514
				50,000	43.73	.5766+e	.3976-e	31,950	1.239	.1253+10	.1153	.9330	.0438	.0470	.0614
60,000	52.48	.8306+e	.4039-e	39,530	1.158	.1803+10	.1248	.8924	.0430	.0482	.0605				

Note: 0.2377-s = 0.2377x10⁻³

TABLE II.- RÉSUMÉ OF SOLUTIONS FOR ELLIPSOIDS

[Mixture composed of 50-percent argon, 40-percent nitrogen, 10-percent carbon dioxide; $\rho_{\infty}/\rho_0 = 10^{-3}$; $p_{\infty} = 2.116 \text{ lb/ft}^2$; $\rho_{\infty} = 0.2377 \times 10^{-5} \text{ slug/ft}^3$, $T_{\infty} = 634^{\circ} \text{ R}$]

V_{∞} , ft/sec	$B_b = 0$				$B_b = 0.5625$				
	A_7	$\frac{R_b}{R_s}$	$\frac{\Delta}{R_s}$	$\frac{\Delta}{R_b}$	A_7	$\frac{R_b}{R_s}$	$\frac{\Delta}{R_s}$	$\frac{\Delta}{R_b}$	
10,000	-0.0293	0.7759	0.0782	0.1008	0.0255	0.8036	0.0784	0.0976	
20,000	-.0243	.8418	.0488	.0580	.0360	.8593	.0489	.0569	
30,000	-.0134	.8424	.0493	.0586	.0517	.8607	.0494	.0574	
40,000	-.0157	.8597	.0456	.0531	.0488	.8765	.0457	.0521	
50,000	-.0173	.8809	.0496	.0562	.0424	.8998	.0496	.0551	
		$B_b = 1.5625$				$B_b = 2.25$			
10,000	.1400	.8530	.0788	.0924	.2140	.8864	.0790	.0892	
20,000	.1725	.8901	.0490	.0550	.2788	.9101	.0491	.0539	
30,000	.1940	.8932	.0495	.0554	.2934	.9174	.0496	.0540	
40,000	.1931	.9058	.0458	.0505	.3027	.9259	.0458	.0495	
50,000	.1778	.9319	.0497	.0533	.2775	.9549	.0498	.0521	

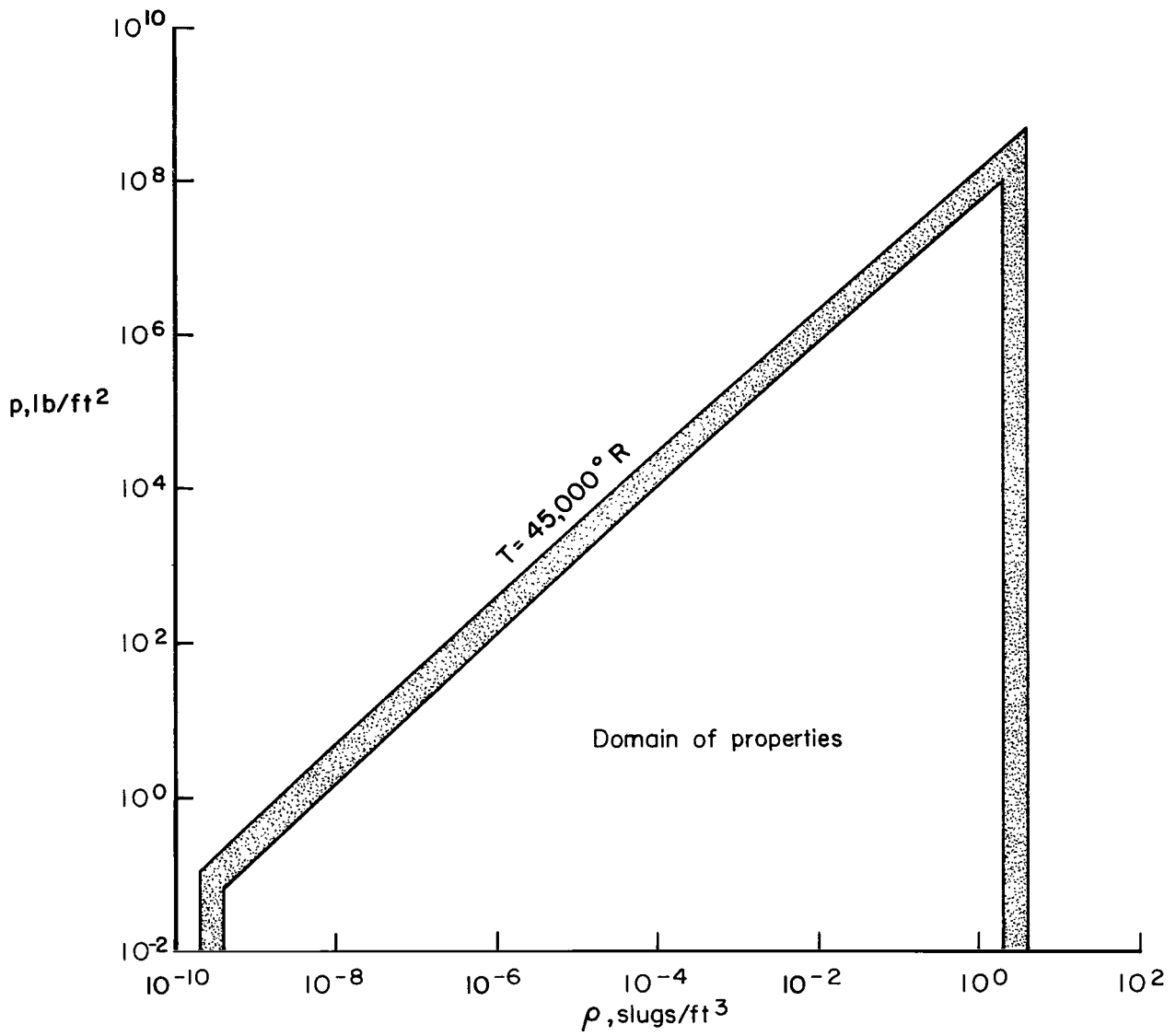
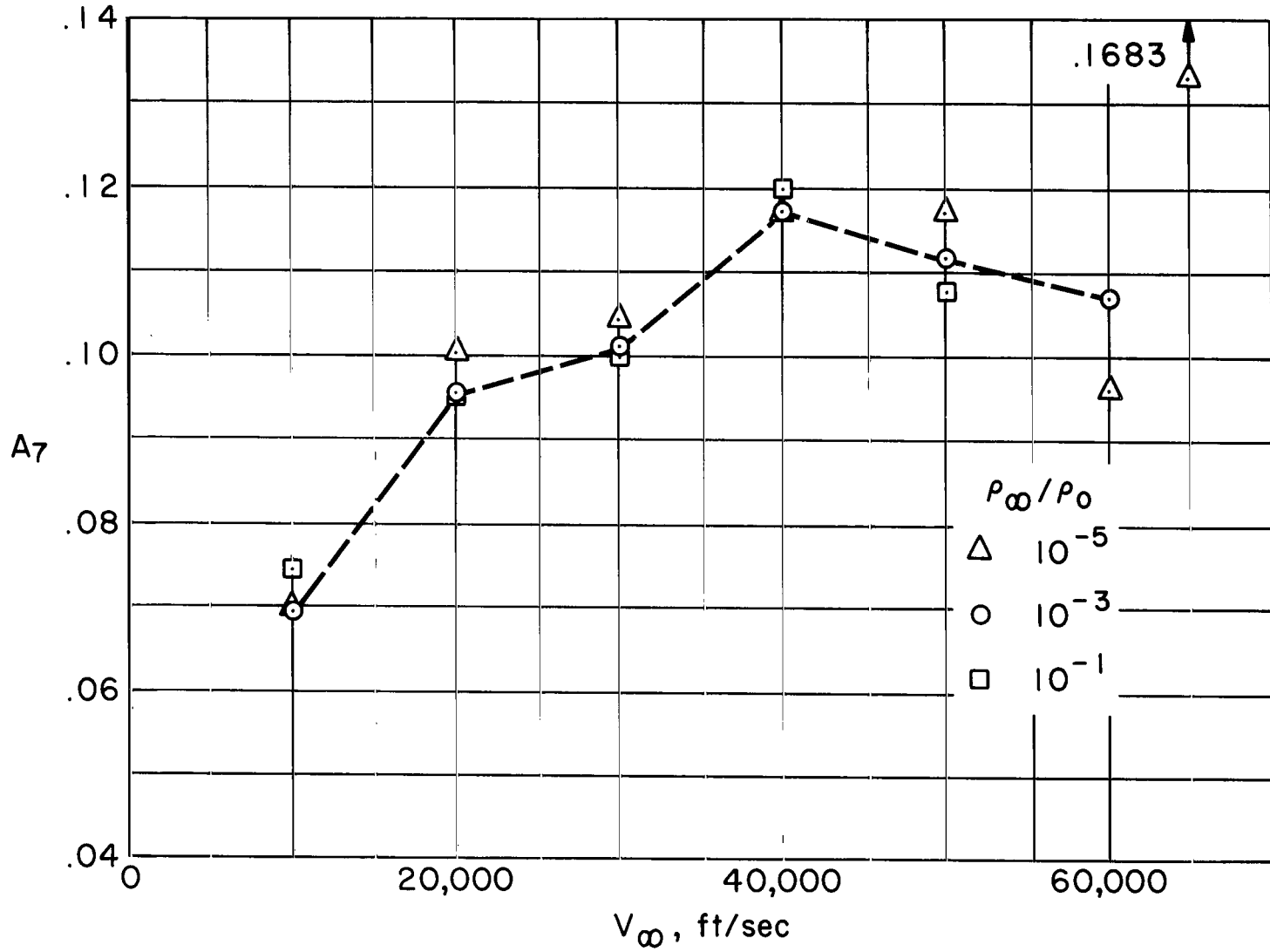
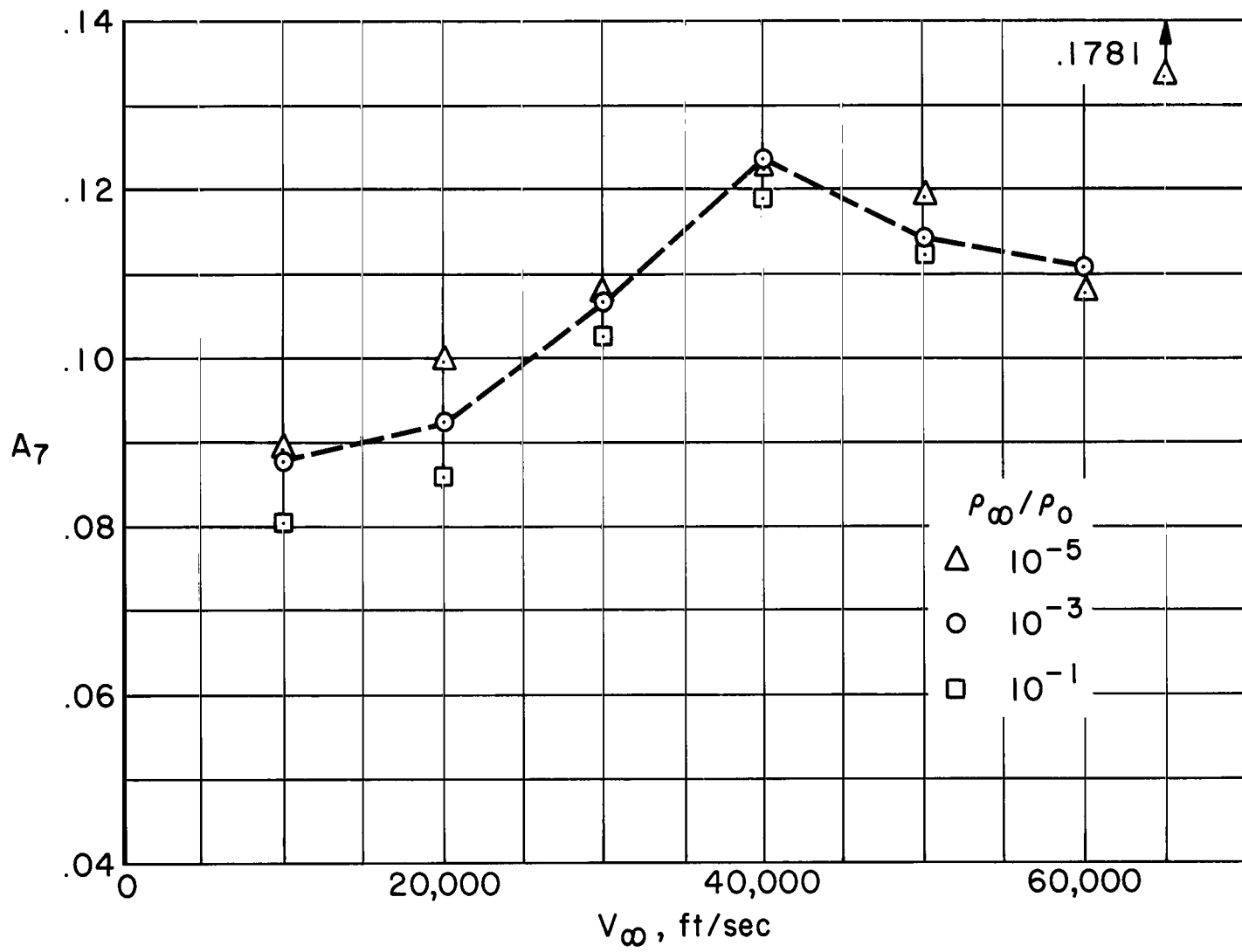


Figure 1.- Domain of thermodynamic properties.



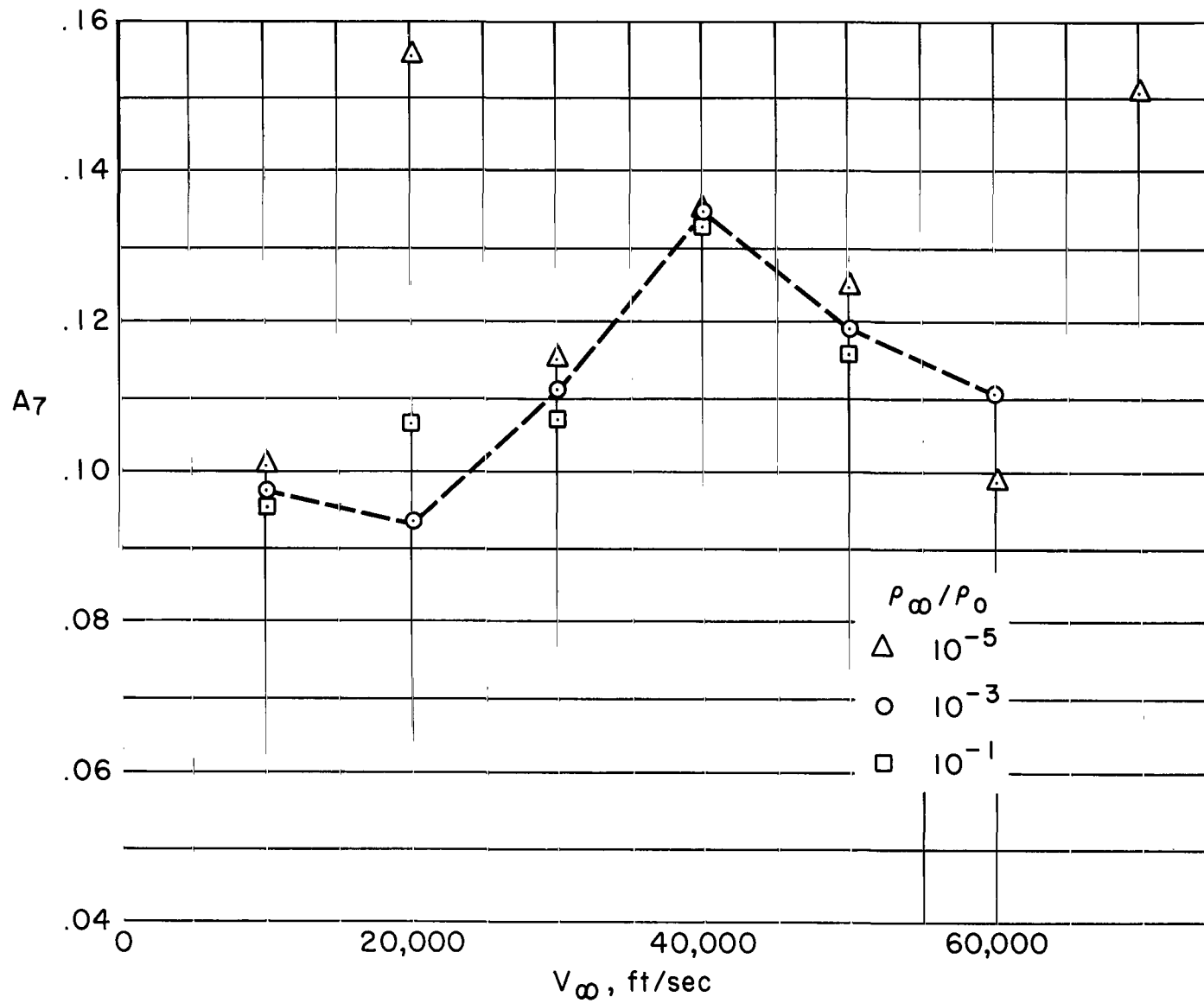
(a) Air, $T_\infty = 514^\circ \text{ R}$.

Figure 2.- Shock-wave parameter for sphere.



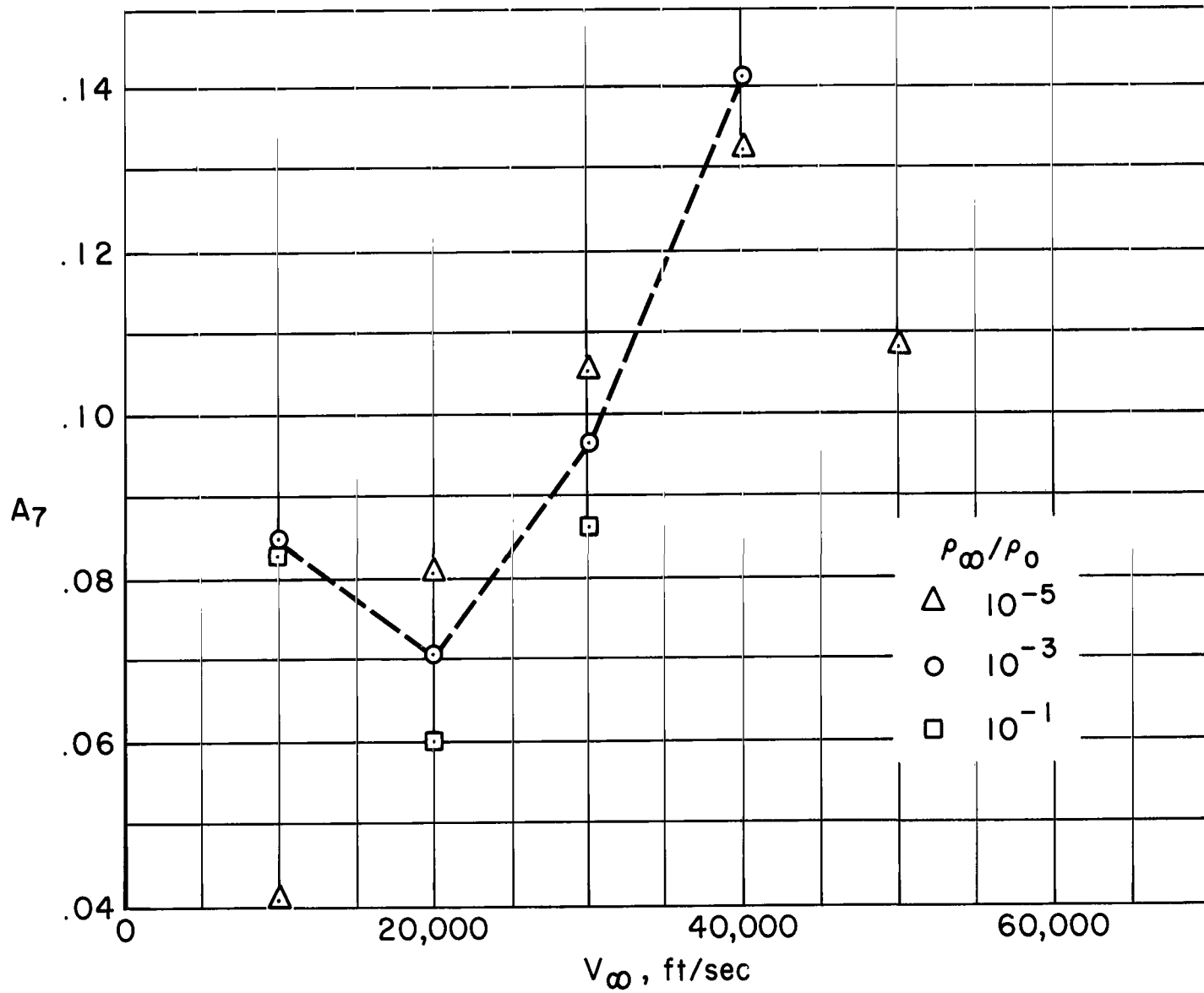
(b) Nitrogen, $T_\infty = 500^\circ \text{R}$.

Figure 2.- Continued.



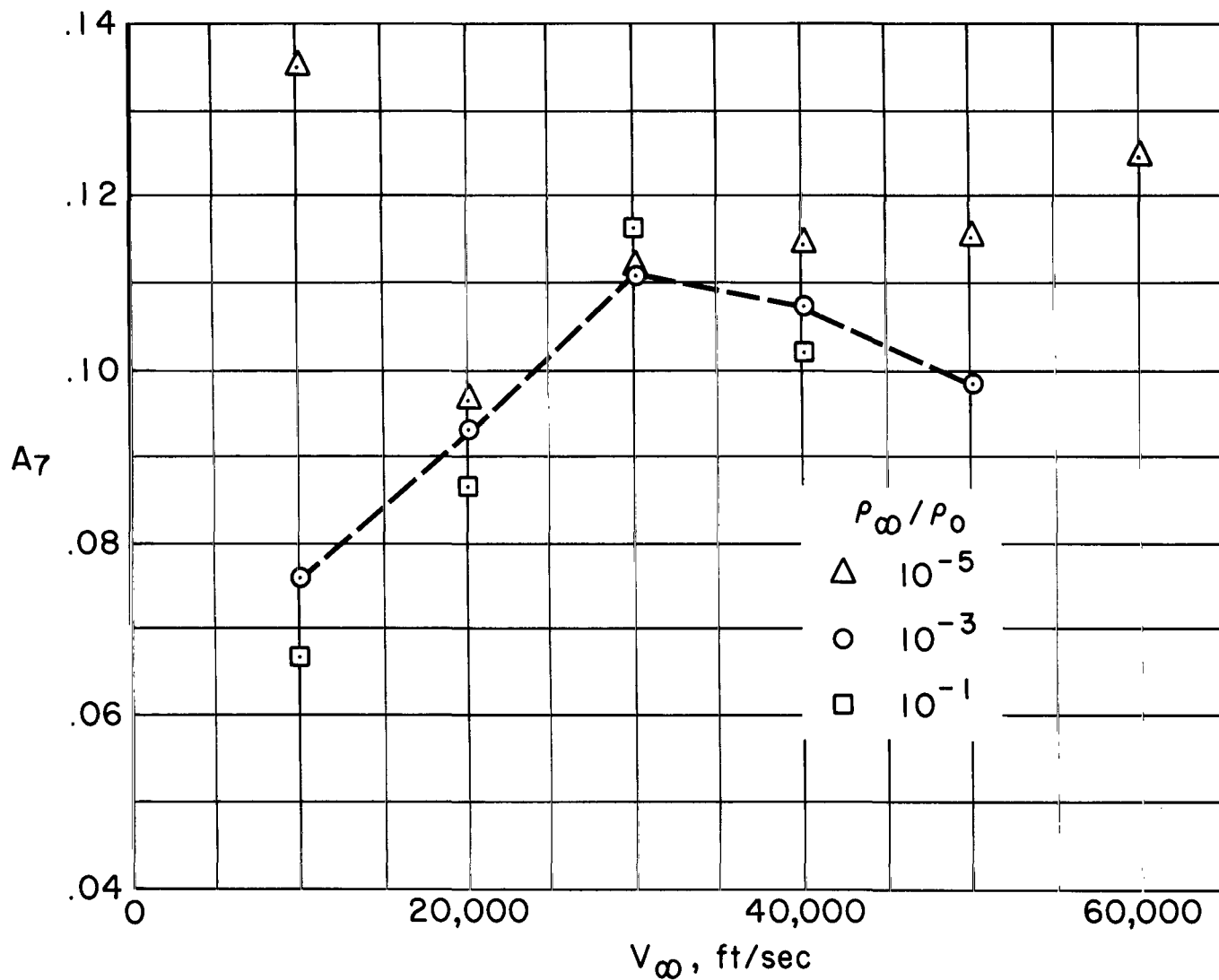
(c) Carbon dioxide, $T_\infty = 784^\circ \text{R}$.

Figure 2.- Continued.



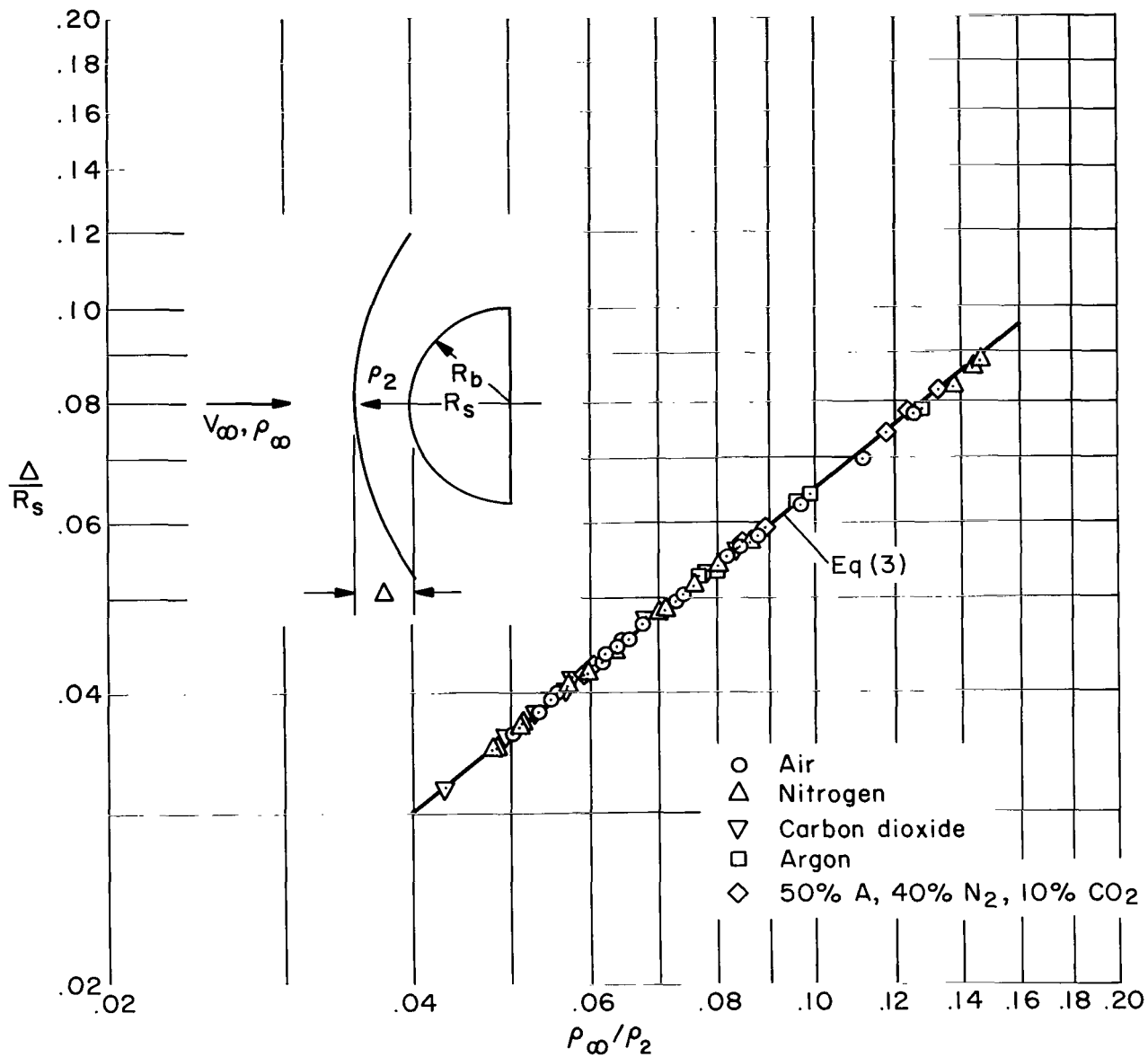
(d) Argon, $T_\infty = 711^\circ \text{ R}$.

Figure 2.- Continued.



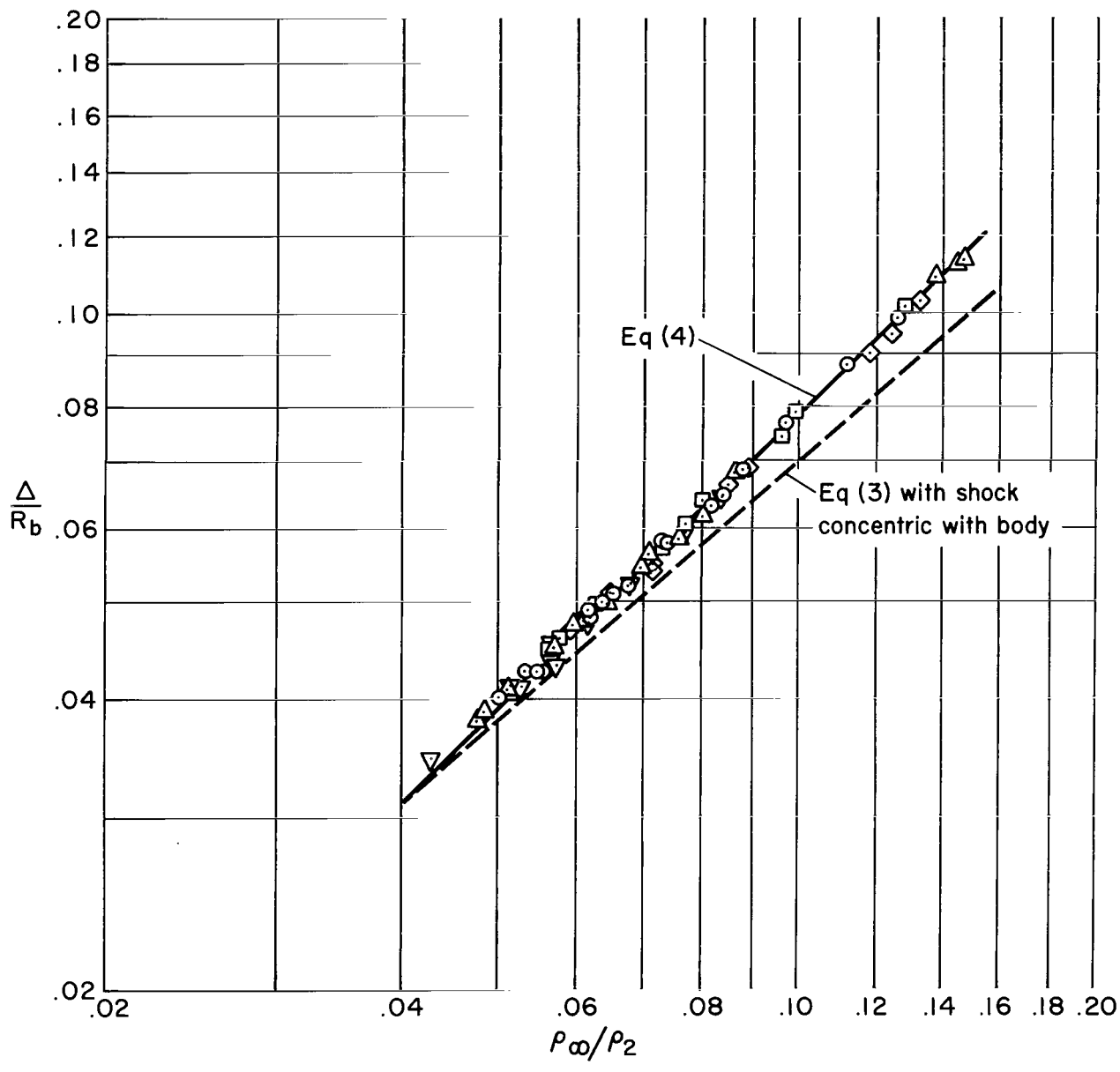
(e) 50-percent argon, 40-percent nitrogen, 10-percent carbon dioxide, $T_\infty = 634^\circ \text{R}$.

Figure 2.- Concluded.



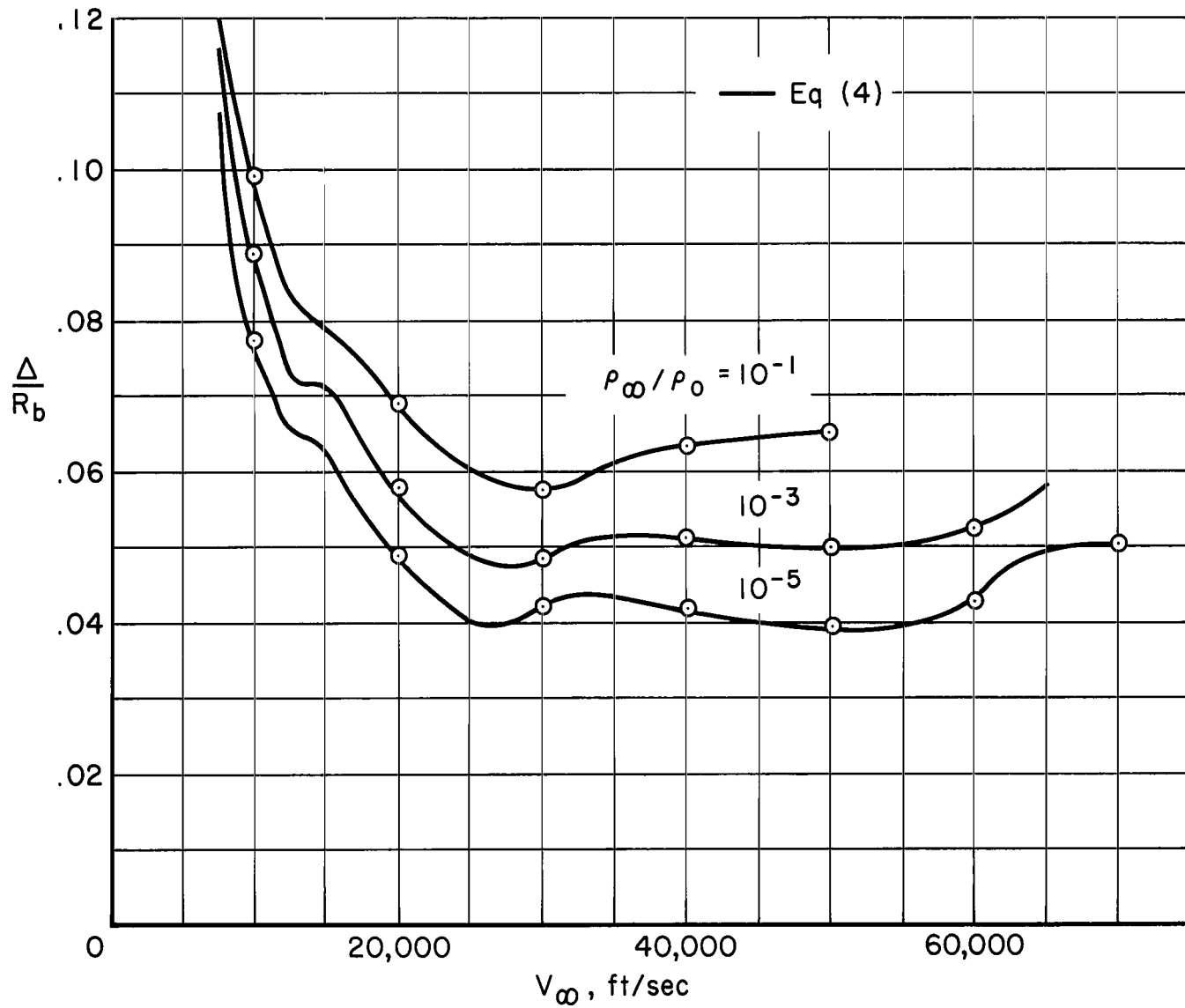
(a) Δ/R_s .

Figure 3.- Shock standoff distance for a sphere as a function of density ratio across normal shock.



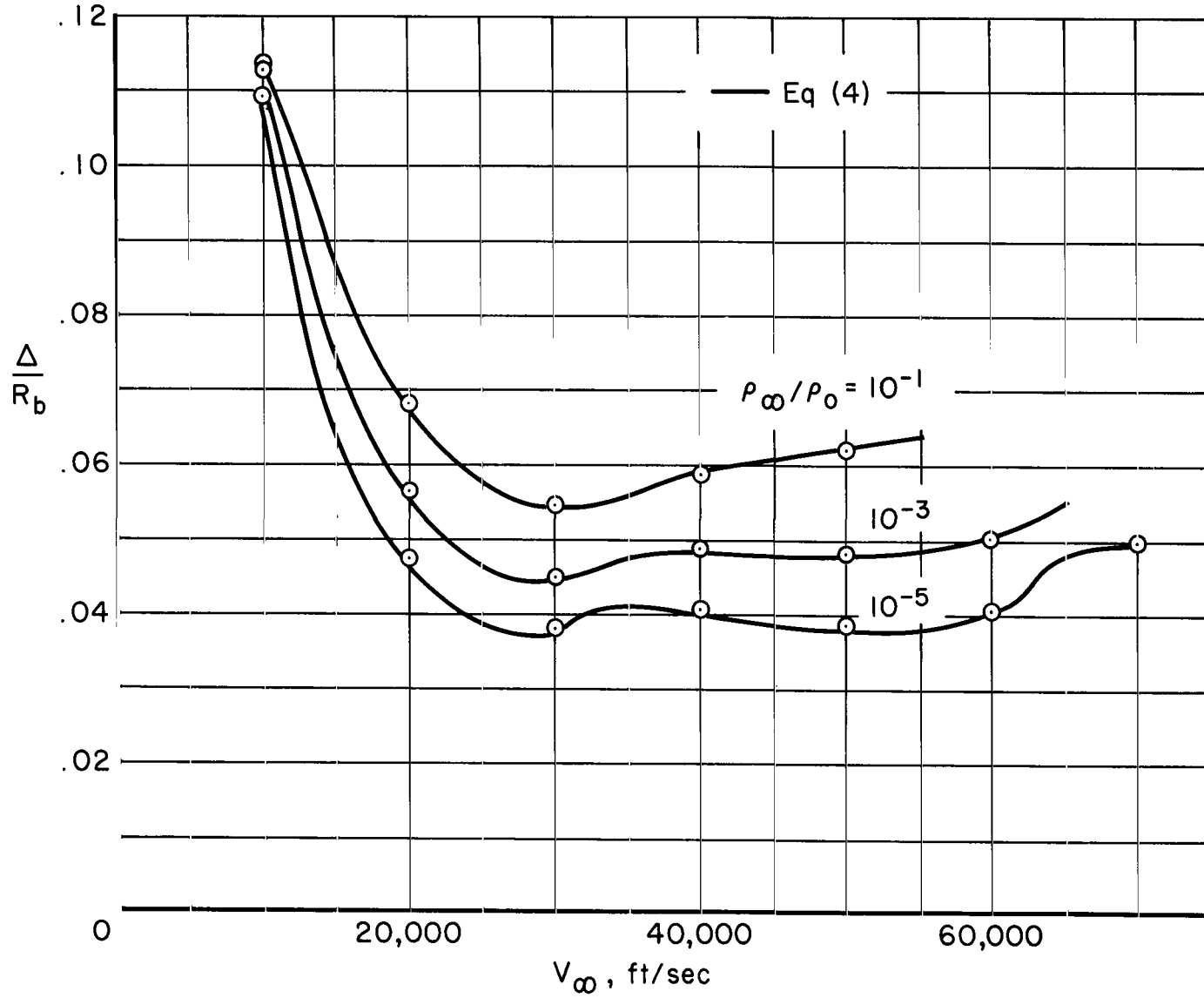
(b) Δ/R_b

Figure 3.- Concluded.



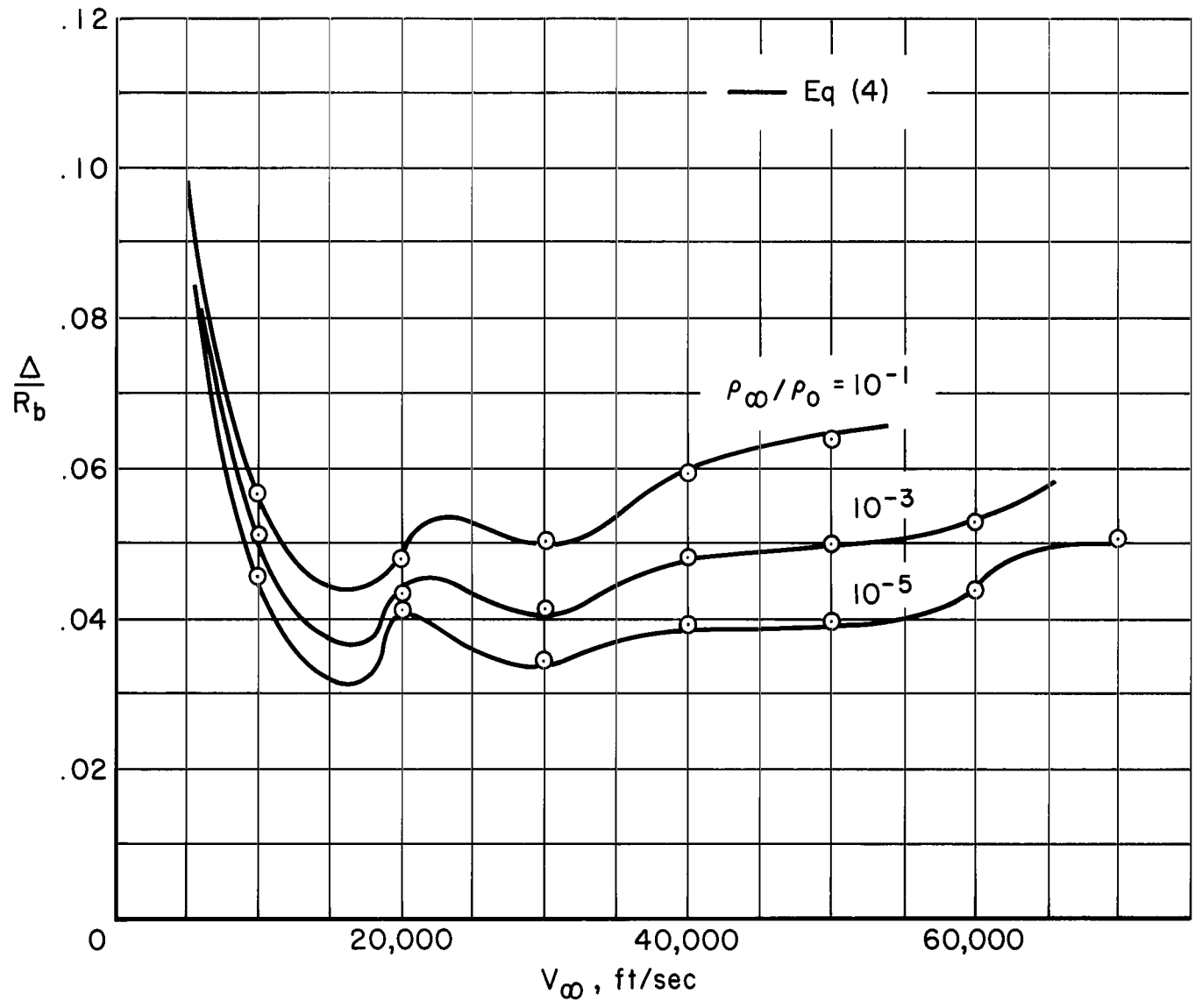
(a) Air, $T_\infty = 514^\circ \text{ R.}$

Figure 4.- Shock standoff distance for a sphere as a function of free-stream velocity and density.



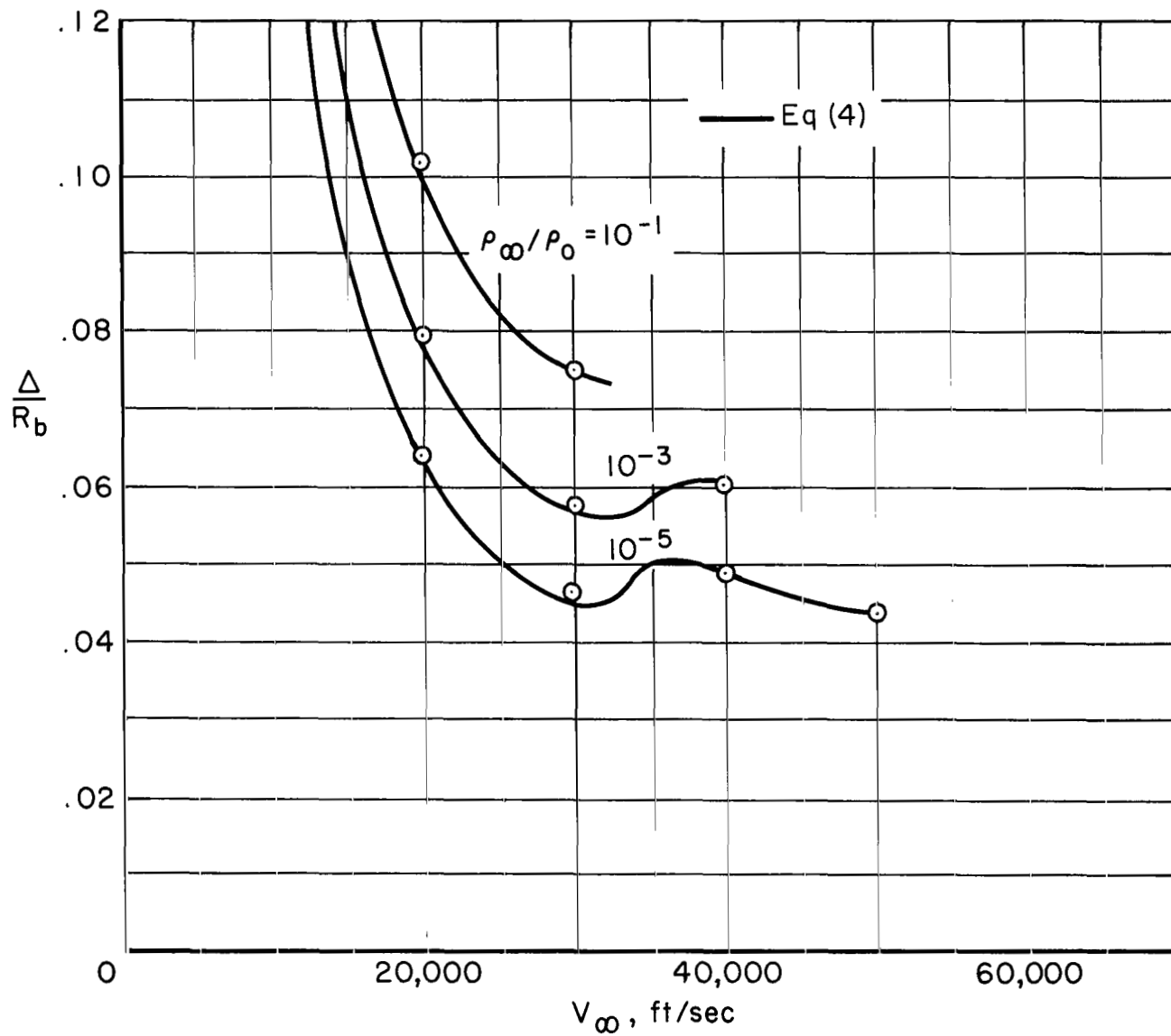
(b) Nitrogen, $T_\infty = 500^\circ \text{ R}$.

Figure 4.- Continued.



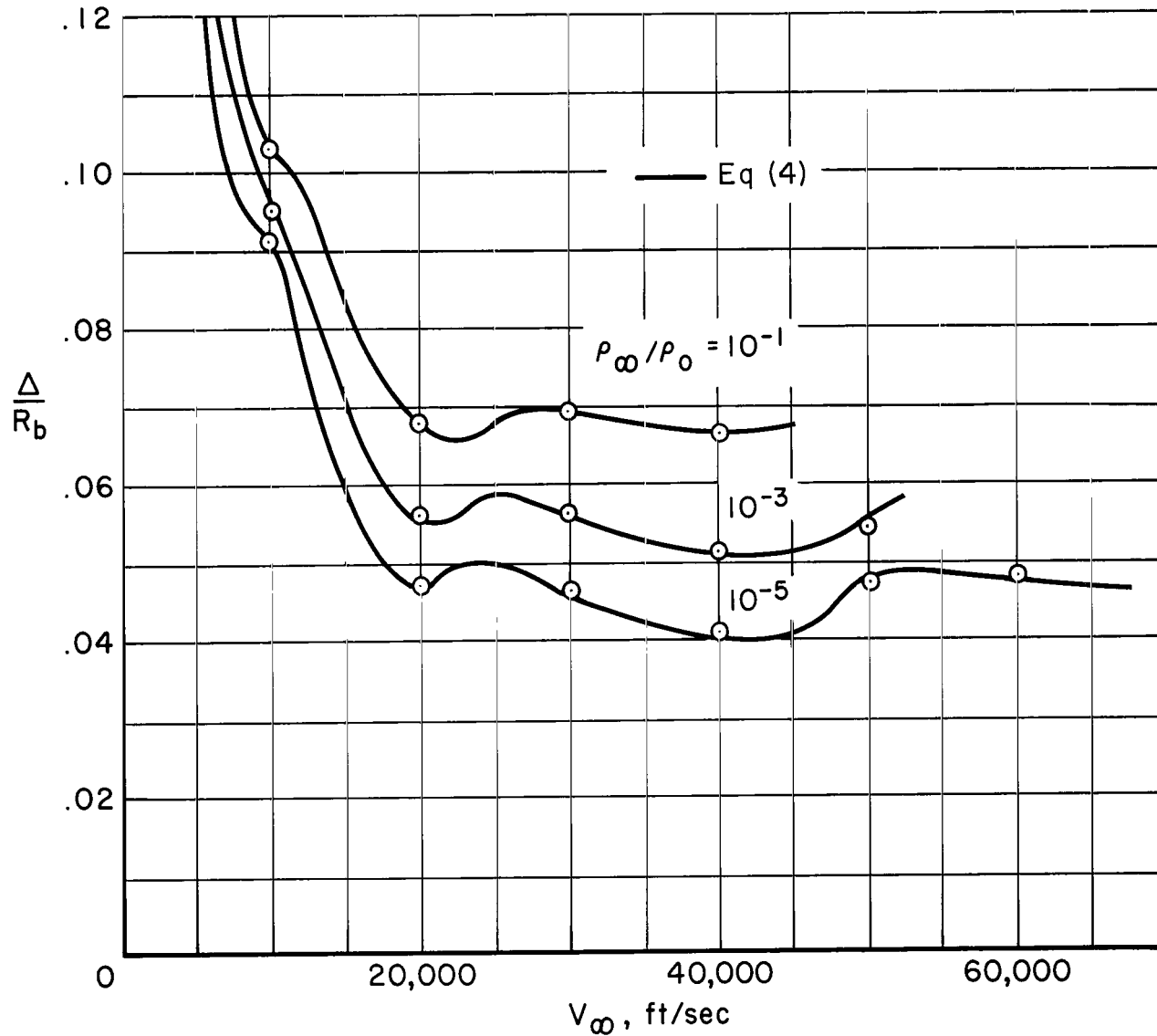
(c) Carbon dioxide, $T_\infty = 784^\circ \text{R}$.

Figure 4.- Continued.



(d) Argon, $T_\infty = 711^\circ \text{ R.}$

Figure 4.- Continued.



(e) 50-percent argon, 40-percent nitrogen, 10-percent carbon dioxide, $T_\infty = 634^\circ \text{ R.}$

Figure 4.- Concluded.

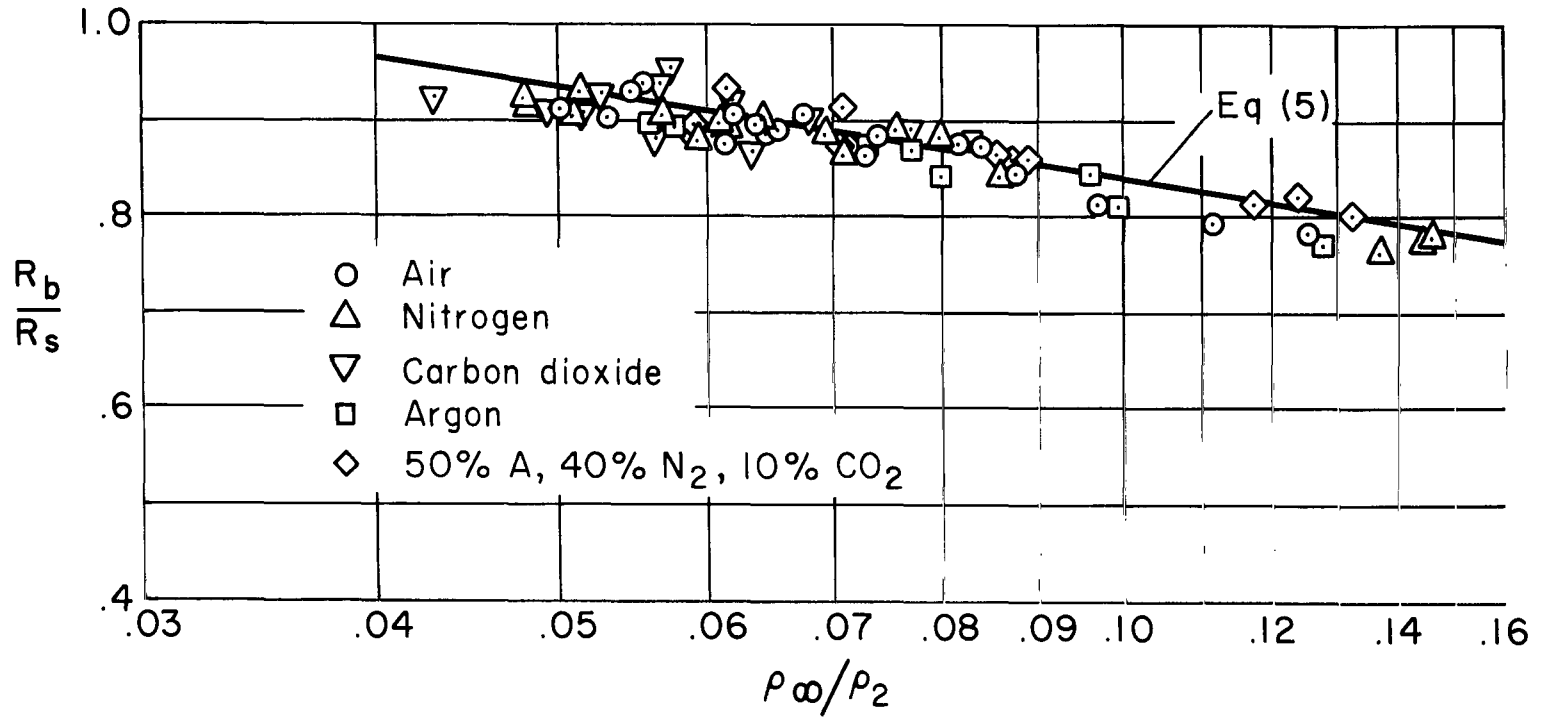


Figure 5.- Ratio of nose radius to shock radius for a sphere as a function of density ratio across normal shock.

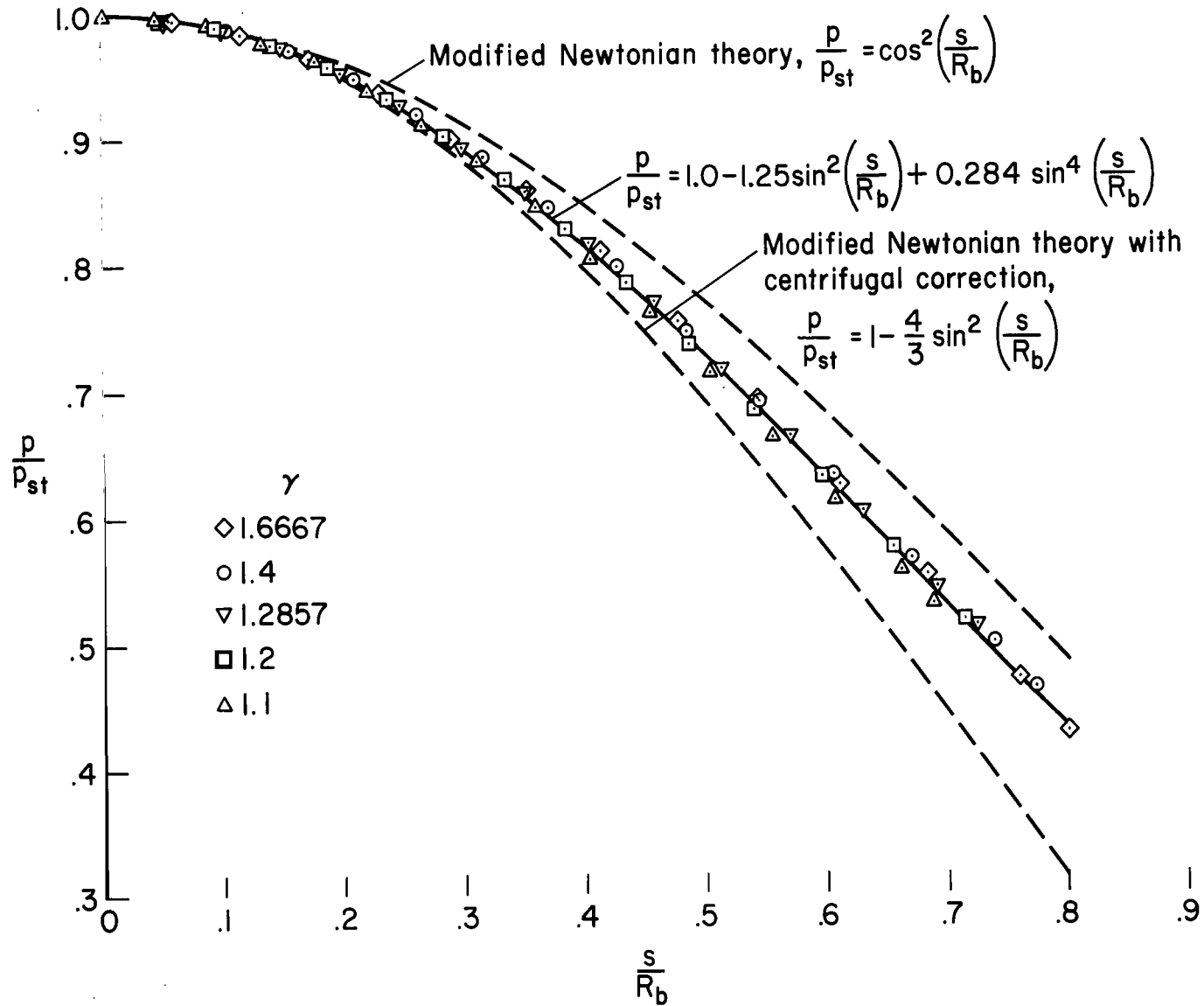


Figure 6.- Effect of γ on surface pressure distribution in subsonic region of spherical nose, perfect gas $M_\infty = 30$.

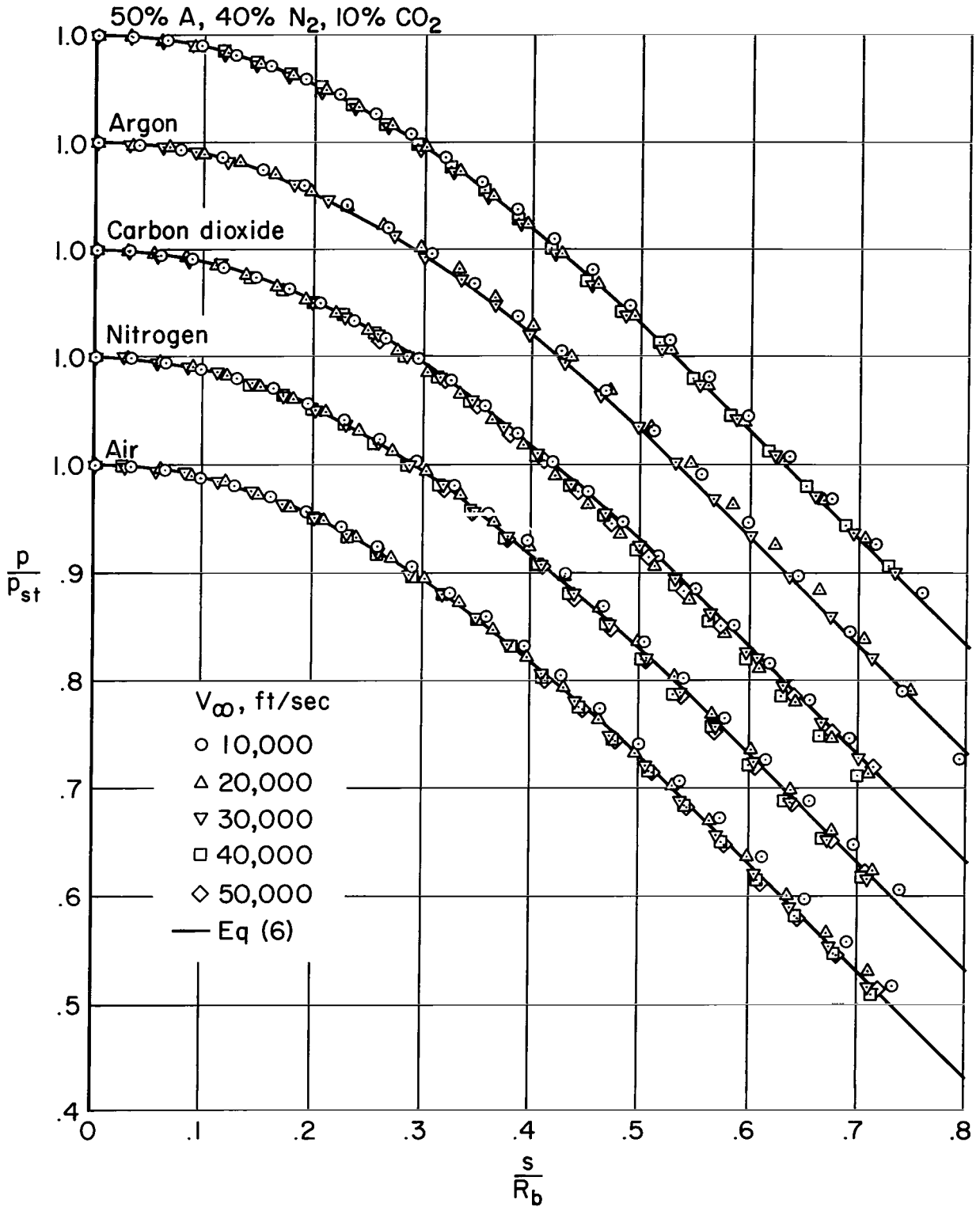


Figure 7.- Surface pressure distribution in subsonic region of spherical nose for real gases, $\rho_\infty/\rho_0 = 10^{-1}$.

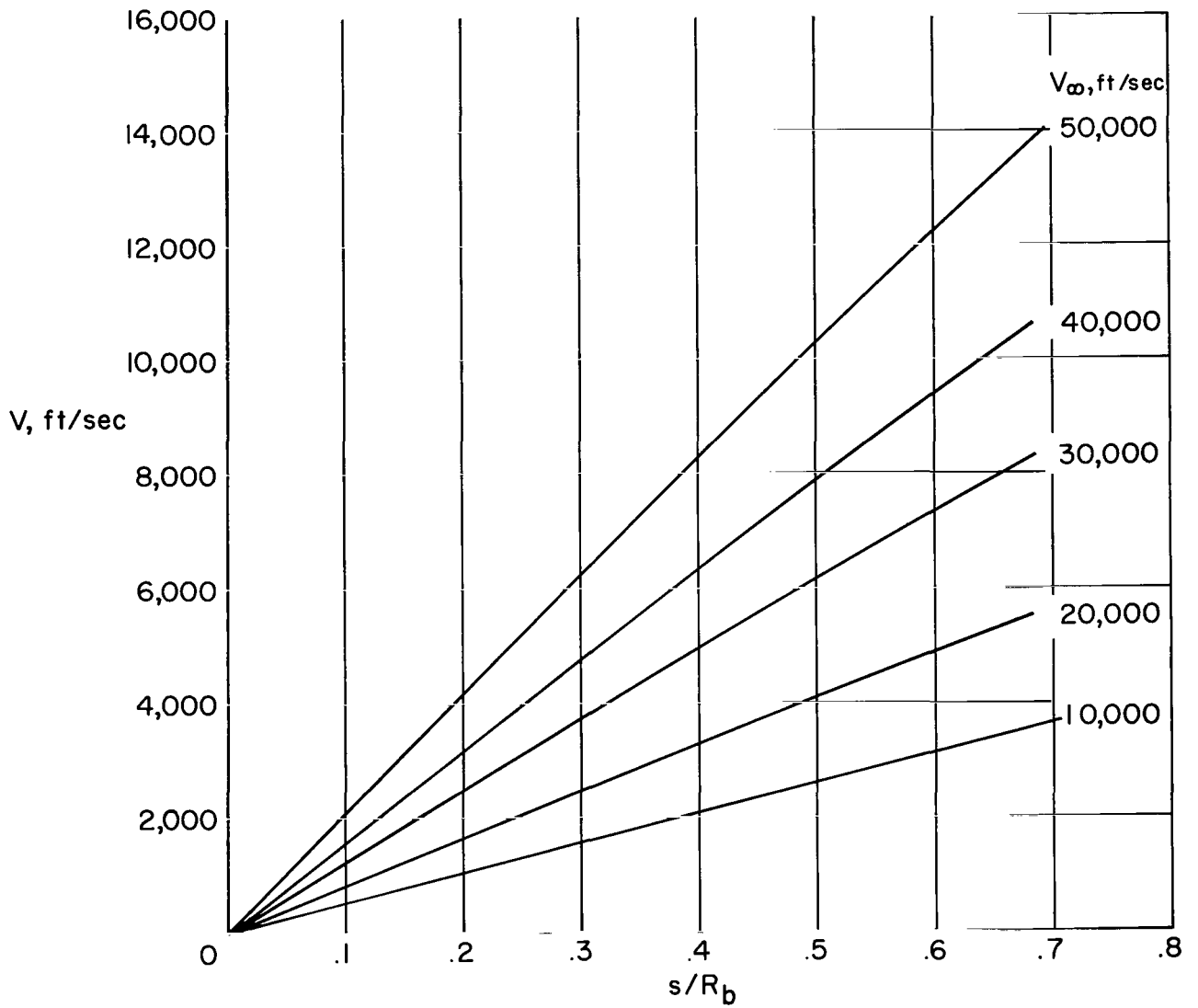


Figure 8.- Velocity distribution in subsonic region of spherical nose for mixture of 50-percent argon, 40-percent nitrogen, and 10-percent carbon dioxide; $T_\infty = 634^\circ \text{ R}$, $\rho_\infty/\rho_0 = 10^{-3}$.

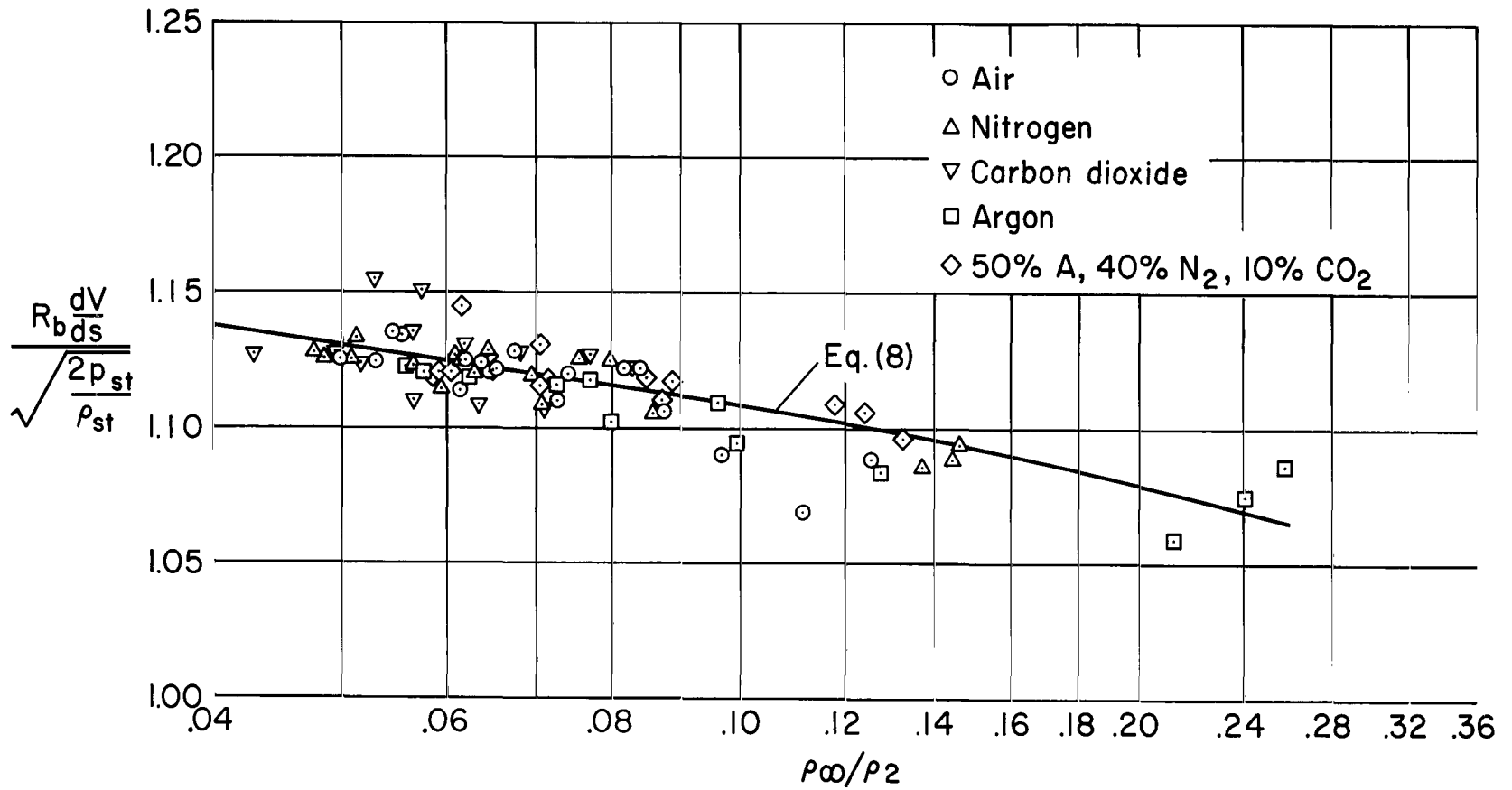


Figure 9.- Stagnation-point velocity gradient for a sphere as a function of density ratio across normal shock.

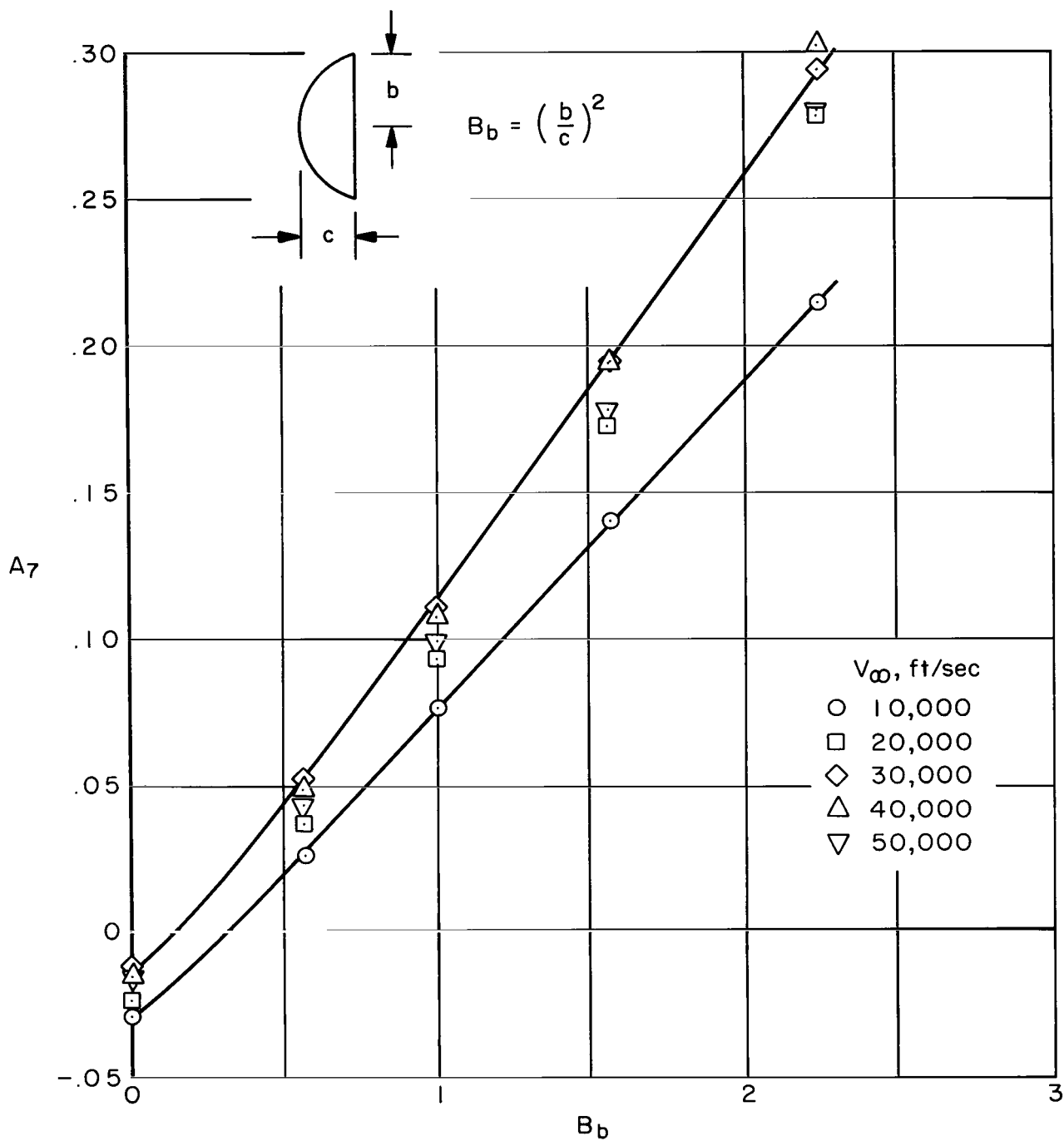


Figure 10.- Shock-wave parameter for ellipsoids in mixture of 50-percent argon, 40-percent nitrogen, 10-percent carbon dioxide; $T_\infty = 634^\circ \text{R}$, $\rho_\infty/\rho_0 = 10^{-3}$.

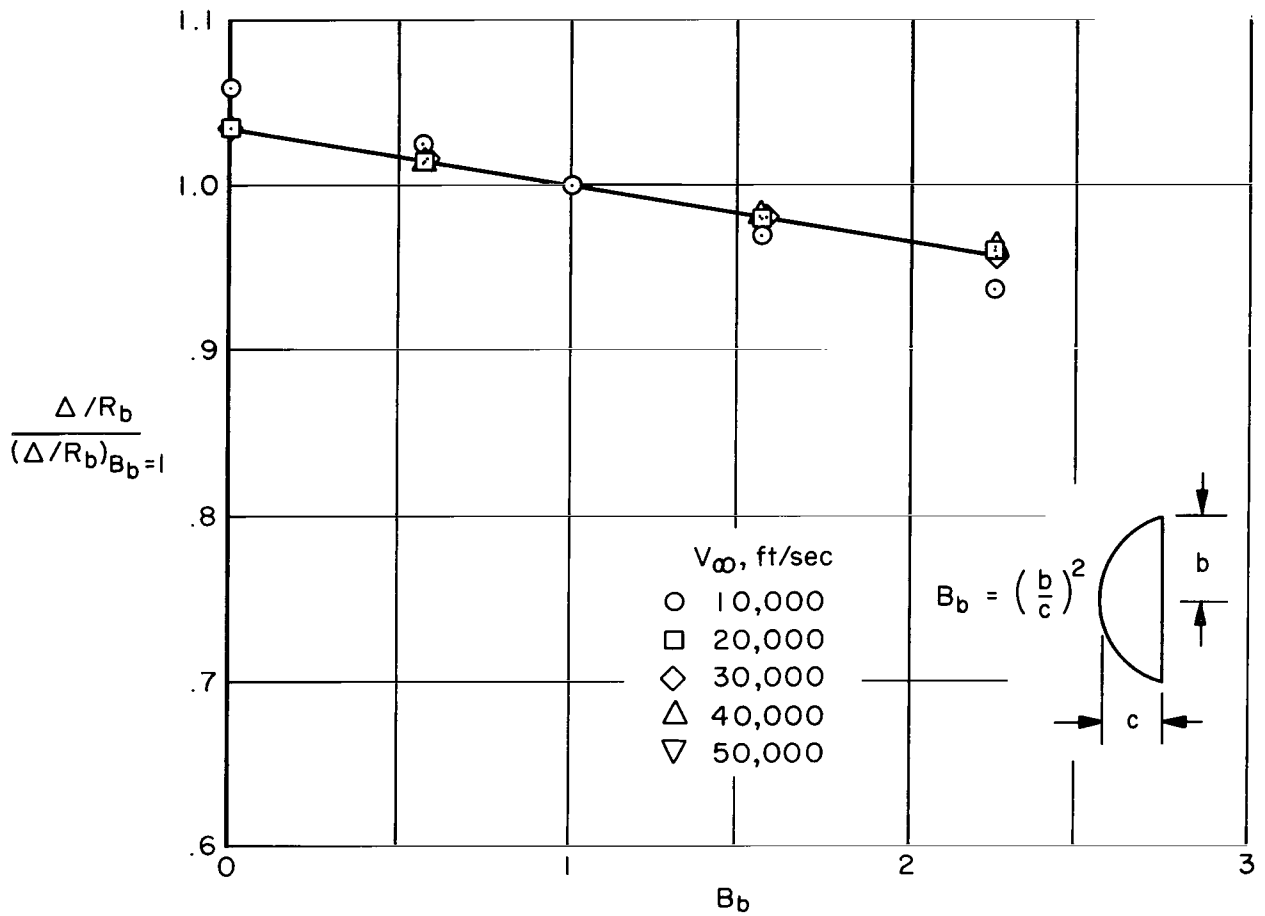


Figure 11.- Shock-wave standoff distance for ellipsoids in mixture of 50-percent argon, 40-percent nitrogen, 10-percent carbon dioxide; $T_\infty = 634^\circ \text{R}$, $\rho_\infty/\rho_0 = 10^{-3}$.

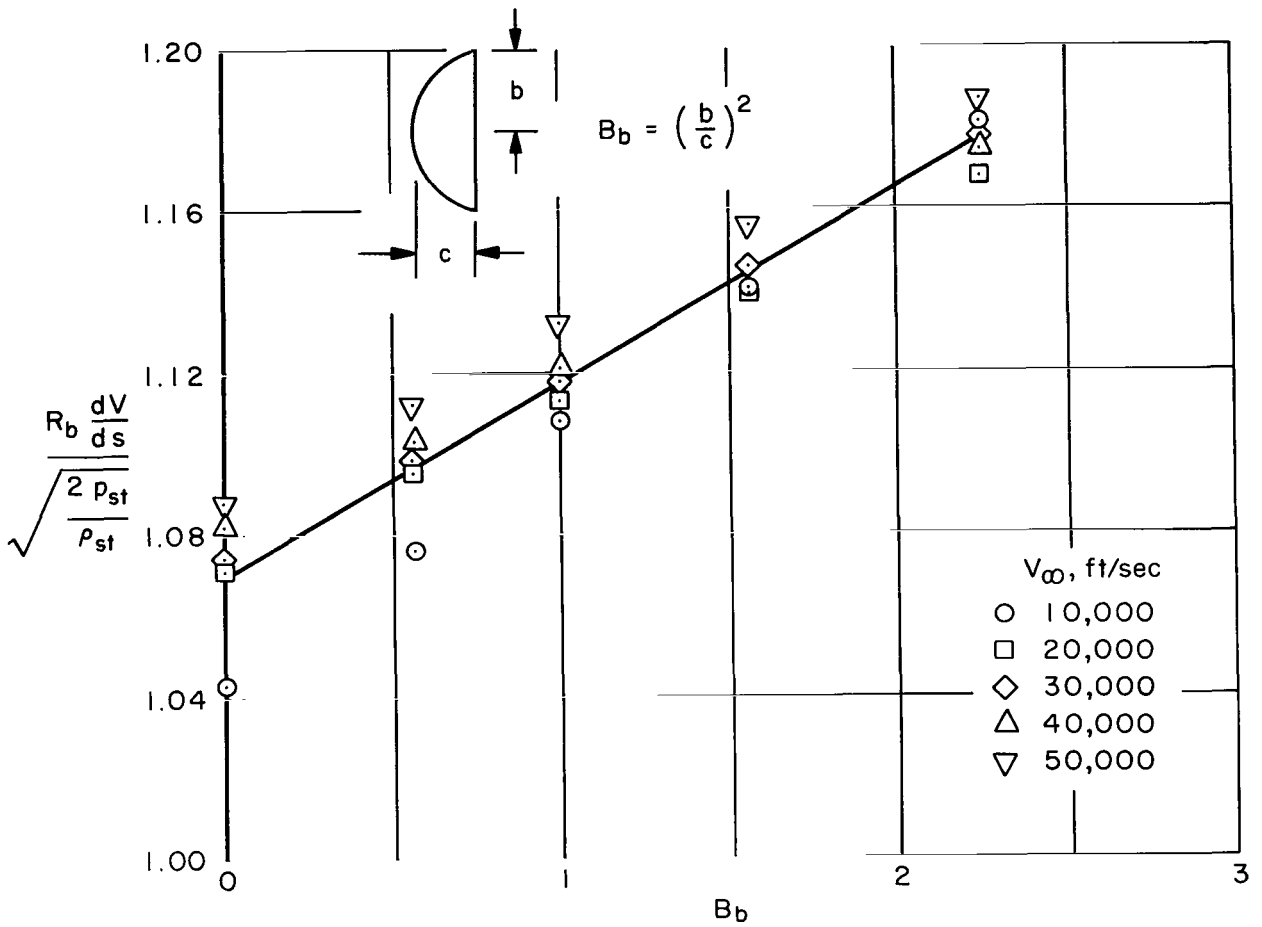


Figure 12.- Stagnation-point velocity gradient for ellipsoids in mixture of 50-percent argon, 40-percent nitrogen, 10-percent carbon dioxide; $T_\infty = 634^\circ \text{R}$, $\rho_\infty/\rho_0 = 10^{-3}$.

2/22/85
5

"The aeronautical and space activities of the United States shall be conducted so as to contribute . . . to the expansion of human knowledge of phenomena in the atmosphere and space. The Administration shall provide for the widest practicable and appropriate dissemination of information concerning its activities and the results thereof."

—NATIONAL AERONAUTICS AND SPACE ACT OF 1958

NASA SCIENTIFIC AND TECHNICAL PUBLICATIONS

TECHNICAL REPORTS: Scientific and technical information considered important, complete, and a lasting contribution to existing knowledge.

TECHNICAL NOTES: Information less broad in scope but nevertheless of importance as a contribution to existing knowledge.

TECHNICAL MEMORANDUMS: Information receiving limited distribution because of preliminary data, security classification, or other reasons.

CONTRACTOR REPORTS: Technical information generated in connection with a NASA contract or grant and released under NASA auspices.

TECHNICAL TRANSLATIONS: Information published in a foreign language considered to merit NASA distribution in English.

TECHNICAL REPRINTS: Information derived from NASA activities and initially published in the form of journal articles.

SPECIAL PUBLICATIONS: Information derived from or of value to NASA activities but not necessarily reporting the results of individual NASA-programmed scientific efforts. Publications include conference proceedings, monographs, data compilations, handbooks, sourcebooks, and special bibliographies.

Details on the availability of these publications may be obtained from:

SCIENTIFIC AND TECHNICAL INFORMATION DIVISION
NATIONAL AERONAUTICS AND SPACE ADMINISTRATION

Washington, D.C. 20546